



RESEARCH ARTICLE

# Spatiotemporal organization and protein dynamics involved in regulated exocytosis of MMP-9 in breast cancer cells

Dominique C. Stephens<sup>1</sup>, Nicole Osunsanmi<sup>1</sup>, Kem A. Sochacki<sup>2</sup>, Tyrel W. Powell<sup>1</sup>, Justin W. Taraska<sup>2</sup> , and Dinari A. Harris<sup>1</sup> 

**Altered regulation of exocytosis is an important mechanism controlling many diseases, including cancer. Defects in exocytosis have been implicated in many cancer cell types and are generally attributed to mutations in cellular transport, trafficking, and assembly of machinery necessary for exocytosis of secretory vesicle cargo. In these cancers, up-regulation of trafficking and secretion of matrix metalloproteinase-9 (MMP-9), a proteolytic enzyme, is responsible for degrading the extracellular matrix, a necessary step in tumor progression. Using TIRF microscopy, we identified proteins associated with secretory vesicles containing MMP-9 and imaged the local dynamics of these proteins at fusion sites during regulated exocytosis of MMP-9 from MCF-7 breast cancer cells. We found that many regulators of exocytosis, including several Rab GTPases, Rab effector proteins, and SNARE/SNARE modulator proteins, are stably assembled on docked secretory vesicles before exocytosis. At the moment of fusion, many of these components are quickly lost from the vesicle, while several endocytic proteins and lipids are simultaneously recruited to exocytic sites at precisely that moment. Our findings provide insight into the dynamic behavior of key core exocytic proteins, accessory proteins, lipids, and some endocytic proteins at single sites of secretory vesicle fusion in breast cancer cells.**

## Introduction

Metastasis is a very complex multicellular process that involves the dissemination of cancer cells from the primary tumor to distant sites and accounts for 90% of human cancer deaths (Weigelt et al., 2005). This hallmark of cancer involves many critical steps, such as the (1) detachment of epithelial cells from the extracellular matrix (ECM), (2) survival within the bloodstream, and (3) growth at the metastatic site (Lu et al., 2011). These cells exocytose extracellular molecules that remodel and break down the structural support of the surrounding ECM, which is made up of a specialized network of fibrous proteins and proteoglycans surrounding many cells. The ECM has many diverse functions, such as providing support, segregating tissues from one another, and regulating intercellular communication (Lu et al., 2011). During metastasis, the ECM is degraded by matrix-degrading proteins called matrix metalloproteinases (MMPs), which are secreted by cells as the result of precisely organized intracellular cell signaling events.

MMPs are a family of zinc- and calcium-dependent proteolytic enzymes that are involved in ECM degradation and have been shown to play important roles in cancer progression (Singh

et al., 2015) by altering cell invasion, migration, metastasis, and tumorigenesis (Llobet et al., 2008; Stetler-Stevenson, 2001; Stetler-Stevenson and Yu, 2001). Studies indicate that increased expression of two homologous MMPs, MMP-9 and MMP-2, correlates with aggressive forms of several cancers, including colorectal cancer, breast cancer, ovarian cancer, and melanoma (Mendes et al., 2005; Saito et al., 2004; Seftor et al., 2001; Zhang et al., 2005). In these cancers, MMP-9 and MMP-2 are secreted by cells, and elevated expression levels have been associated with poor prognosis in patients. The overwhelming evidence suggesting the importance of MMP secretion in the progression of many types of cancers has led to the use of these enzymes as prognostic markers of metastatic cancers (Sakata et al., 2004).

Secretion of these MMPs relies on the coordinated trafficking of secretory vesicles (or secretory granules) containing the MMPs, followed by regulated exocytosis from cells. In exocytosis, membrane-bound secretory vesicles are carried to the cell membrane, and their contents are secreted into the extracellular environment. This secretion is possible because the vesicle transiently fuses with the outer cell membrane (Jahn and

<sup>1</sup>Department of Chemistry, Howard University, Washington, DC; <sup>2</sup>Laboratory of Molecular Biophysics, National Heart, Lung, and Blood Institute, National Institutes of Health, Bethesda, MD.

Correspondence to Dinari A. Harris: [dinari.harris@howard.edu](mailto:dinari.harris@howard.edu).

© 2019 Stephens et al. This article is distributed under the terms of an Attribution–Noncommercial–Share Alike–No Mirror Sites license for the first six months after the publication date (see <http://www.rupress.org/terms/>). After six months it is available under a Creative Commons License (Attribution–Noncommercial–Share Alike 4.0 International license, as described at <https://creativecommons.org/licenses/by-nc-sa/4.0/>).

Fasshauer, 2012; Jahn et al., 2003) through a series of spatially coordinated and precisely timed fusion or exocytic events. These events include vesicle trafficking, vesicle docking, vesicle priming, vesicle fusion, and vesicle recapture (Sudhof, 2004). Dysfunctional release of secretory vesicle cargo can lead to diseases such as diabetes, as well as a range of neuropathologies and cancer (Graczyk and Rickman, 2013). The molecular mechanisms that control exocytosis in all these diseases have been of considerable interest for decades, and studies have uncovered many different groups of proteins that are involved at discrete steps in exocytosis.

For instance, as it relates to exocytosis and cancer, dysregulation of the class of small GTPases and Rab effector proteins, such as Rab27a and Rab27b isoforms, Rab25, Rab40b, and Rabphilin, has been shown to promote tumor cell migration, invasion, and metastasis through disruption of membrane vesicle trafficking and docking (Gomi et al., 2007; Hendrix et al., 2010b; Shaughnessy and Echard, 2018; Tzeng et al., 2017; Tzeng and Wang, 2016; Wang et al., 2017). The soluble N-ethylmaleimide-sensitive factor (NSF) attachment protein receptors, soluble NSF attachment protein receptor (SNARE) proteins, and SNARE modulators have long been implicated in vesicle trafficking and fusion in synaptic nerves. However, more recent evidence suggests a role of SNAREs in tumor invasion and metastasis in cancer cells through trafficking of MMPs, SNAP23, vesicle-associated membrane protein 3 (VAMP3), VAMP7, syntaxin-13, and syntaxin-4. All of these have been shown to be involved in secretion of various types of MMPs, degradation of ECM, and tumor cell invasion (Kean et al., 2009; Sun et al., 2016; Williams et al., 2014). Additionally, many proteins classically associated with endocytosis have also been implicated in human cancers and exocytosis pathways. Abnormal expression or mutations in endocytic proteins, including the dynamins and related proteins, can enhance cancer cell proliferation, tumor invasion, and metastasis (Haferlach et al., 2010), presumably through regulation of the fusion and vesicle recapture (Anantharam et al., 2011; Llobet et al., 2008; Min et al., 2007; Samasilp et al., 2012; Trexler et al., 2016; Tsuboi et al., 2004).

Studies suggest that vesicle trafficking of MMPs is a crucial factor in the regulation of ECM degradation and cancer progression (Schnaeker et al., 2004). While much of this information was gathered through protein interactions identified through traditional biochemical methods, a comprehensive understanding of their spatial organization and temporal dynamics during exocytosis of secretory vesicles containing MMPs is lacking in live cells. Because of this lack of spatiotemporal information, as it relates to cancer progression and metastasis in cancer cells, the role these exocytic (and endocytic) proteins play and the local dynamics of these proteins at sites of exocytosis of MMPs are unclear. Therefore, there is a need to visualize the dynamic behavior of many of these proteins at sites of exocytosis to fully understand the complexity (in time and space) in the assembly and regulation of the exocytic machinery at sites of fusion and release of MMPs.

Here, we used TIRF microscopy to map the spatiotemporal organization and dynamics of proteins involved in secretory vesicle trafficking of MMP-9 and regulated exocytosis in MCF-7

breast adenocarcinoma cells. Specifically, two-color TIRF was used as an imaging-based screening tool to systematically identify the relative correlation (colocalization) of proteins with secretory vesicles containing MMP-9, as well as the recruitment or loss of many of these proteins at subsequent exocytic sites. This method identified several key protein “functional” groupings that are involved during steps in the trafficking and exocytosis of MMP-9 from secretory vesicles in cancer cells, including several Rab proteins and Rab effector proteins, SNARE and SNARE modulator proteins, and some classic endocytic proteins. Our data indicate that several of these proteins are localized at exocytic sites before fusion and diffuse away after exocytosis, while others are only transiently recruited to exocytic sites during the time of fusion. Collectively, our data provide important insight into the local spatial organization and temporal dynamics of proteins before, during, and after membrane fusion of secretory vesicles containing the protumor marker MMP-9 and its release from MCF-7 breast cancer cells. These results provide a unified systems-level, steady-state, spatial map of the protein landscape of individual exocytic structures associated with MMP-9 secretion.

## Materials and methods

### Plasmids, solutions, and cells

MCF-7 cells were maintained in Dulbecco’s modified Eagle’s medium without phenol red (10% fetal bovine serum, 1% penicillin-streptomycin, 11.1 mM glucose, 10 mM HEPES, 2 mM glutamine, and 1 mM pyruvate) at 37°C at 5% CO<sub>2</sub>. For experiments, cells were plated on 25-mm collagen-coated coverslips. Cells were transfected using 1 µg of each plasmid with Lipofectamine 2000 according to the manufacturer’s instructions and imaged 24–48 h after transfection. All imaging was performed at 28°C in imaging buffer (10 mM HEPES, 130 mM NaCl, 2.8 mM KCl, 5 mM CaCl<sub>2</sub>, 1 mM MgCl<sub>2</sub>, and 10 mM glucose at pH 7.4). Exocytosis was stimulated by serum starving transfected cells for 1 h followed by a 30-min induction with 500 nM PMA before imaging. Chemicals were from Sigma-Aldrich, cell culture reagents and Lipofectamine were from Life Technologies, and fixatives were from Electron Microscopy Sciences.

### TIRF microscopy

TIRF microscopy was performed as previously described (Trexler et al., 2016). Briefly, an inverted fluorescence microscope (IX-81; Olympus) with a 100×/1.45-numerical-aperture objective (Olympus) was used for TIRF imaging. Fluorescence was excited alternatively with 488-nm or 561-nm laser lines that were combined and passed through a 488/561DM filter cube (Semrock). Emission was spectrally separated using a 565DCXR dichroic mirror and projected side by side on an electron multiplying charge-coupled device electron multiplying charge-coupled device camera (DU 897; Andor) with a DualView image splitter (Photometrics) containing 525Q/50 and 605Q/55 filters. The green and red images were superimposed in postprocessing by acquiring an image of 100-nm yellow-green beads (Invitrogen) that were visible in both channels, mapping the

position of six beads in both channels, and then superimposing the channels using projective image transform. This protocol was performed each day, and the image transform was used to superimpose cell images. Images were acquired with IQ2 software (Andor) successively in the green then red channels with an exposure time of 500 ms and a 500-ms pause between pairs of images. Pixel size was 160 nm.

### Image analysis

All analysis was performed using custom Matlab scripts and ImageJ. Correlation analysis was performed as previously described (Larson et al., 2014). All of the local maxima above a user-defined threshold and >2  $\mu\text{m}$  away from the edge of the cell boundary were identified in each whole-cell green image (MMP9-GFP). Each local maximum was centered in a 4  $\mu\text{m}$   $\times$  4  $\mu\text{m}$  cropped region. These cropped regions from several cells were each normalized to the brightest pixel and averaged together. The regions corresponding to the green local maxima were also excised from the red images, normalized to the brightest pixel, and averaged together. In each average red image, 12 radial line scans were taken and averaged together. Randomly selected regions equal in number to the excised regions were processed in the same way. The average random line scan was then subtracted from the average red image line scan to account for background intensity statistics. The peak height for each construct was determined by measuring the maximum intensity difference between the first point (center of the image) and all other points in the averaged scan. Smaller 1.0  $\mu\text{m}$   $\times$  1.0  $\mu\text{m}$  cropped, vesicle-centered, red/green regions were used to calculate Pearson's  $c$  for each green peak:

$$c = \frac{\sum_{i=1}^n (G_i - G)(R_i - R)}{\sqrt{\sum_{i=1}^n (G_i - G)^2} \sqrt{\sum_{i=1}^n (R_i - R)^2}}$$

where  $G_i$  and  $R_i$  represent pixel intensities in the two channels and  $G$  and  $R$  indicate average pixel intensity. The region size was chosen based on the spacing of secretory vesicles in an attempt to capture only one structure per correlation region on average. Correlations were then averaged together, yielding an average  $c$  for each construct. Correlation values were calculated between peak-centered green excised regions and randomly selected red regions as well.

Exocytic events were analyzed by hand selecting event coordinates and stack position in the green channel in ImageJ. Matlab scripts extracted a raw intensity mean ( $F_{\text{center}}$ ) from a 480-nm square box centered on the coordinates and a mean background value from a 1,440-nm square surround area ( $F_{\text{surround}}$ ); this was performed for both channels. The traces were then temporally aligned to the frame before the maximum intensity decrease of the MMP9-GFP channel ( $t = 0$  in our trajectories). We aligned to the maximum intensity decrease because this was the most robust feature of MMP9-GFP signal at exocytic events. At the time resolution used here, the transient brightening of MMP9-GFP is always observed followed by the rapid decrease of fluorescence intensity in all traces. Individual trajectories were background subtracted and normalized over 0 to 1 by:

$$\text{Normalized fluorescence} = \frac{[(F_{\text{center}} - F_{\text{surround}}) - F_{\text{min}}]}{F_{\text{max}} - F_{\text{min}}}$$

where  $F_{\text{min}}$  is the minimum fluorescence intensity over the  $F_{\text{center}}$  background-subtracted trace and  $F_{\text{max}}$  is the maximum. Average trajectories and standard errors were calculated from the normalized trajectories.

For all correlation analysis and analysis of exocytic events, 15 cells were imaged from cotransfections with the MMP-GFP and a red fluorescently labeled protein. For these experiments, a single coverslip with cells cotransfected with MMP9-GFP and a red-labeled protein was imaged.

### Immunofluorescence and siRNA

Cells were transfected with SMARTpool small interfering RNA (siRNAs; Dharmacon, GE Healthcare Life Sciences) against Rab27a (5873) or Rab27b (5874) according to the manufacturer's instructions using Lipofectamine 2000. Cells were cultured with siRNAs for 24–72 h before imaging experiments. For immunofluorescence, cells were fixed with 2% paraformaldehyde (PFA) in imaging buffer for 20 min at room temperature. Cells were permeabilized with 0.5% Triton X-100 for 2 min and then incubated in blocking buffer (3% bovine serum albumin and 0.2% Triton X-100 in PBS) for 1 h at room temperature or overnight at 4°C. Primary antibodies for MMP-9 (1:50; sc-21733), Rab27a (1:200, sc-136995; Santa Cruz Biotechnology), or Rab27b (1:200, ab76779; Abcam) were added to samples in blocking buffer for 1 h at room temperature or overnight at 4°C. Samples were washed and incubated with secondary antibodies (anti-rabbit or anti-goat Alexa Fluor 647-conjugated secondary antibodies, 1:1,000) for 30 min before washing and postfixing for 20 min at room temperature in 2% PFA. siRNA depletion was estimated from images by measuring mean fluorescence intensity in whole-cell regions in siRNA-transfected cells versus non-transfected cells in the same field of view.

### Western blotting

For detection of secreted MMPs in conditioned media, cells treated without and with PMA were done as parallel sets of cultures. Conditioned media containing one of the MMPs (MMP-9, MMP-2, or MMP-1) were collected and filtered by a 0.22- $\mu\text{m}$  syringe filter to exclude any cell debris before concentrating using Amico Ultra centrifugal (Millipore) concentrators. For overexpression studies of Rab27 isoforms, cells transfected with either Rab27a or Rab27b were compared with controls (no transfection). These parallel sets of cultures were done in triplicate before harvesting. Cells were harvested, pelleted, and lysed with incubation in RIPA buffer (1% Nonidet P-40, 0.5% sodium deoxycholate, and 0.1% SDS in PBS with Complete Protease inhibitor tablet [Roche] and 100  $\mu\text{M}$  phenylmethylsulfonyl fluoride added) for 30 min on ice with intermittent vortexing. Cell debris was pelleted by centrifuging the lysate at 15,000 rpm for 10 min. Conditioned media protein or lysate protein content was quantified with a bicinchoninic acid assay (BCA-1; Sigma-Aldrich), and 20  $\mu\text{g}$  of protein was loaded per lane on a 10–20% Tris-Glycine Novex gel (Invitrogen). The gel was transferred to a polyvinylidene fluoride membrane and blocked in 10%

Omniblock in Tris-buffered saline with 0.2% Tween-20 overnight at 4°C. Blots were incubated in primary antibody (MMP-9, 1:500, sc-21733; MMP-2, 1:200, sc-13594; MMP-1; 1:200, sc-21731; actin, 1:1,000, sc-1615) for 1 h at room temperature, washed, and incubated in secondary antibody (MMP-9, MMP-1, MMP-2 [anti-mouse, 1:2,500], Rab27a [anti-mouse, 1:2,000], Rab27b [anti-rabbit, 1:2,000], and actin [anti-goat, 1:5,000]) before extensive washing and treatment with enhanced chemiluminescence kit and exposure to film. All bands from Western blot were quantified using ImageJ software (National Institutes of Health). For quantification all band intensities were measured and averaged from three separate experiments.

## EM

For thin-section transmission EM (TEM), cells were fixed in 2.5% glutaraldehyde and 1% PFA for 20 min at room temperature. Secondary fixation with 1% osmium and staining with 1% uranyl acetate was performed before dehydration and infiltration with epon LX-112. 80-nm sections were made and imaged on a JEOL 1400 TEM with an AMT XR-111 camera (Advanced Microscopy Techniques).

For CLEM, cells were plated on standard coverslips as described above, transfected with MMP9-GFP, and processed 1 day later. Cells were rinsed briefly in stabilization buffer (70 mM KCl, 30 mM HEPES, 5 mM MgCl<sub>2</sub>, and 3 mM EGTA, pH 7.4) twice and then unroofed by sonication in 2% PFA in stabilization buffer. Sonication was performed within 10 s after being placed in PFA with a Branson Sonifier 450 (1/8-inch tapered tip, 5 mm above the coverslip, single 300-ms pulse, and lowest output setting). Cells were fixed for 20 min in 2% PFA. After fixation, cells were stained for 1 h with phalloidin-Alexa Fluor 647 (Invitrogen) according to the manufacturer's instructions. TIRF microscopy was used to image a 15 × 15 image montage of a large field of unroofed cells. After fluorescence imaging, the coverslips were marked with a diamond objective marker and fixed in 2% glutaraldehyde in PBS overnight at 4°C. They were stained with freshly made 0.1% tannic acid for 20 min, rinsed thoroughly in water, stained with 0.1% uranyl acetate for 20 min, rinsed again, and then dehydrated with increasing concentrations of ethanol (5 min each of 15%, 30%, 50%, 70%, 80%, 90%, and 3 × 100%). The coverslips were then critical-point dried with a Tousimis Samdri-795. The samples were cut down to the area of interest with a diamond scribe and coated with platinum-carbon and carbon in a JEOL JFD-V freeze fracture device. The platinum-carbon was rotary coated at 17 degrees, and the carbon was coated at 90 degrees.

The replica was lifted from the coverslip with 5% hydrofluoric acid and placed onto a 75-mesh copper TEM grid coated with Formvar and carbon. TEM was performed in a JEOL 1400 using SerialEM software to create montages at a magnification of 15,000×. The phalloidin fluorescence image was used to map the fluorescence image onto the EM image in Adobe Photoshop. This allowed correlation of MMP9 fluorescence to specific vesicles. The coordinates of three MMP9-positive vesicles in fluorescence and EM were used to quantitatively map the fluorescence image onto the EM image using a nearest-neighbor two-dimensional affine transformation in Matlab. This

maintains the pixel information from the original fluorescence image rather than interpolating to get an artificially smoothed fluorescence image.

## Online supplemental material

Fig. S1 shows endogenous MMP-9 protein expression levels in MCF-7 cells and the release (exogenous) of MMP-9 from these same cells following regulated exocytosis. Fig. S2 provides a more detailed view of the two-color colocalization pattern used in Fig. 2, as well as snapshots and quantification of dynamic change in fluorescence of proteins and lipids at exocytic sites of MMP9-GFP used in Figs. 4, 5, 6, 7, 8, and 9. Figs. S3 and S4 further characterize the role the two distinct Rab27 isoforms, Rab27a and Rab27b, have in MCF-7 cells. Table S1 shows the correlation values, error, standard deviation, and details about the plasmids and source obtained during the screening of colocalized proteins with secretory vesicles containing MMP-9.

## Results

### Secretory vesicles contain MMP-9 near the plasma membrane of MCF-7 cells

To image the spatiotemporal organization associated with trafficking of secretory vesicles and regulated exocytosis of MMPs in cancer cells, we transiently expressed MMP-9 tagged with green fluorescent protein (GFP) in MCF-7 breast cancer cells. Images using TIRF, with this MMP-9 recombinant fusion protein (MMP9-GFP), revealed many secretory vesicles containing the marker in MCF-7 cells (Fig. 1A). The large number of MMP9-GFP observed in vesicles is consistent with its routine use to mark secretory vesicles in cancer cells (Kean et al., 2009). To get a detailed examination of the spatial organization of secretory vesicles containing MMP-9 and their relative distribution at the plasma membrane, we used correlative light and electron microscopy (CLEM) on cells transfected with MMP9-GFP (Fig. 1B). The advantage of CLEM is that it combines both light microscopy and EM, allowing for images that can be used to identify cellular structures (e.g. secretory vesicles) in whole-cell images (via light microscopy) on top of a more detailed higher-resolution image (via EM) of specific regions of a cell (Heuser 2000; Sochacki et al., 2012).

Plasma membrane sheets were imaged with TIRF and subsequently prepared for TEM by platinum coating. The resulting fluorescence associated with secretory vesicles containing MMP9-GFP can be seen in the whole-cell TIRF image (Fig. 1B; left). Platinum replicas were then imaged, and the TEM image (Fig. 1B; center) was aligned to give the merged image (Fig. 1B; right). In the magnified merged image in Fig. 1C (right), those punctate structures observed with MMP9-GFP in the TIRF image (Fig. 1C; left) overlay very well with the secretory vesicles seen in the higher-resolution TEM image (Fig. 1C; middle). CLEM images of unroofed plasma membranes revealed a variety of secretory vesicles located near the plasma membrane, in addition to a dense network of cortical actin surrounding those vesicles. Many of the membrane-associated secretory vesicles visible by EM are labeled with various amounts of MMP9-GFP. This includes some vesicles showing no apparent GFP labeling

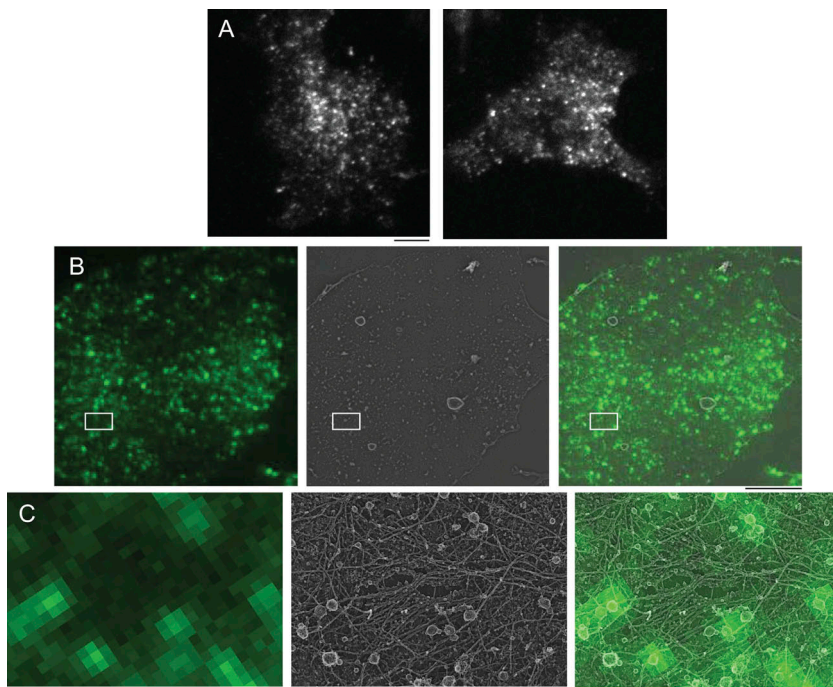


**Figure 1. Secretory vesicles containing MMP9-GFP near the plasma membrane of MCF-7 cells. (A)** Two representative TIRF images of MCF-7 cells transfected with MMP9-GFP. Scale bar, 5  $\mu$ m. **(B)** Images from CLEM microscopy: TIRF image of MMP9-GFP (green) from a MCF-7 cell (left), platinum replica TEM image (gray) of the same MMP9-GFP transfected MCF-7 cell (middle), and overlay of TIRF MMP9-GFP image and platinum replica TEM image (merged) of an unroofed MCF-7 cell plasma membrane sheet (right). Scale bar, 5  $\mu$ m. **(C)** Enlarged regions (box in B) from CLEM microscopy (scale bar, 300 nm; same order as in B). Note the presence of other unlabeled membrane structures found on the MCF-7 cell membrane (e.g., actin filaments are visible all around the secretory vesicles).

and suggests a variety of secretory vesicles types in cancer cells (Corcoran, Wilson, and Kirshner 1984). The size ( $112 \pm 26$  nm;  $n = 75$ ) and shape (small and spherical) of these secretory vesicles are consistent with measurements made previously in the same cell line (Vic et al., 1982). These data indicate that MMP9-GFP is a reliable marker of secretory vesicles in MCF-7 cells.

#### Imaging-based screen identifies proteins associated with secretory vesicles containing MMP-9

Next, we used two-color TIRF as a screening tool to map the association of a library of proteins ( $\sim 150$  recombinant proteins) to sites of secretory vesicles containing MMP-9 across the plasma membrane of MCF-7 cells. We quantitatively determined their relative association or colocalization after we transiently expressed MMP9-GFP and coexpressed a second red-labeled (mCherry, mRFP, dsRed, or mKate) protein of interest in the same cells (Fig. 2, A–C). The red-labeled recombinant proteins we chose were known to have a variety of biological roles and functions, including cellular trafficking, membrane trafficking, signal transduction, exocytosis, endocytosis, ECM degradation, adhesion, and cytoskeletal elements. This approach has been used previously to successfully map the spatial organization and temporal dynamics at single sites of exocytosis of neuropeptide Y (NPY) from dense core vesicles (DCVs) in both neuroendocrine PC12 cells and endocrine INS-1 cells, insulin secreting beta cell derived line (Larson et al., 2014; Trexler, Sochacki, and Taraska 2016), as well as the vesicular acetylcholine transporter from small synaptic-like microvesicles (SLMVs) in PC12 cells (Somasundaram and Taraska 2018).

This imaging-based screening method relies on transient transfection of cells with fluorescently tagged proteins. This method enabled rapid screening of a large subset of proteins, which would not have been feasible using lower-throughput methods such as genome-engineered cell lines (Ran et al.,

2013a,b). Furthermore, transient expression allowed us to visualize dynamics that might otherwise be difficult to detect at lower expression levels under either endogenous or lower-expression promoter control. Overexpression can be problematic, however, as protein levels could affect protein localization, dynamics, or other cellular behaviors. To test for possible overexpression effects on our analysis, we confirmed by using nine correlated proteins that there was no relationship between expression and correlation values (data not shown). Similar effects were also seen using the neuronal secretory granule marker NPY-GFP in PC12 cells (Larson et al., 2014) and INS-1 cells (Trexler et al., 2016). With these experimental caveats in mind, the TIRF-based screen helped us identify key proteins and lipids that can specifically localize to secretory vesicle containing MMP-9. However, we cannot fully exclude the possibility that the native behavior of the proteins could be modulated by expression levels or fluorescent tagging.

For the colocalization analysis, we determined the steady-state correlation values for just  $>150$  red-labeled proteins and analyzed thousands of secretory vesicles containing MMP9-GFP from MCF-7 cells (Table S1). We observed a range of patterns of associations with exocytic structures, like those reported on DCVs, in PC12 and INS-1 cells (Larson et al., 2014; Somasundaram and Taraska, 2018; Trexler et al., 2016). In general, we observed three distinct groups of colocalizations: (1) associated (colocalized), (2) no relationship (not specifically colocalized), and (3) excluded (not colocalized). The first group of associations observed are those proteins that showed high associations or colocalization (e.g., Rab27b; Fig. 2, A–C) with secretory vesicles containing MMP9-GFP. Within this “associated” group, we see a large range of correlation values (Fig. 2 D), presumably due to the complex, dynamic, and possibly heterogeneous nature of secretory vesicles, as well as to the diversity of proteins surveyed (Taylor et al., 2011). The second group of

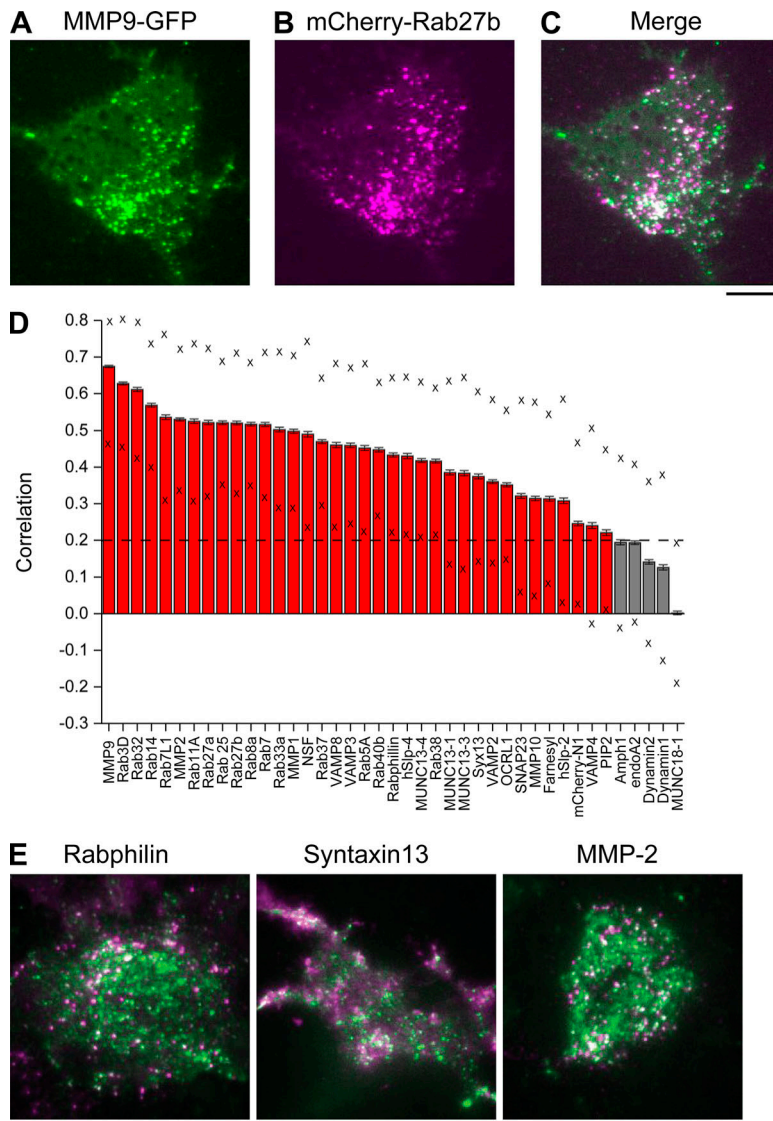


**Figure 2. Correlation analysis with MMP9-GFP measures protein colocalization with secretory vesicles in MCF-7 cells. (A–C)** TIRF images of an MCF-7 cell cotransfected with MMP9-GFP (A) and mCherry-Rab27b (B). **(C)** Merged image. Scale bar, 10  $\mu$ m. **(D)** Shown is the correlation analysis of 42 proteins with MMP9-GFP-labeled secretory vesicles in MCF-7 cells. Cells are sorted based on their mean correlation values and compared with the control (MMP9-mCherry), which showed the highest correlation value. Red boxes indicate proteins associated with secretory vesicles, and gray boxes indicate proteins that are nonspecifically associated or not associated with secretory vesicles. The whiskers are the standard error, and the  $\times$  marks above and below each dataset are the standard deviations. **(E)** Representative TIRF images from the correlation analysis from the various categories of proteins associated with secretory vesicles, including merged images of MMP9-GFP, with Rabphilin-mCherry (Rab effector proteins), syntaxin13-mCherry (SNARE proteins), or MMP2-mCherry (other luminal secretory vesicle cargo). For all correlation assays using two-color TIRF, 15 cells were imaged from cotransfections with the MMP-GFP and a red fluorescently labeled protein. A single coverslip with cells cotransfected with MMP9-GFP and a red-labeled protein was imaged. Scale bar, 10  $\mu$ m.

proteins showed no relationship with exocytic structures (e.g., dynamin1; Fig. S2) and mainly showed nonspecific associations with secretory vesicles. The third group of proteins was “excluded” and was never associated with secretory vesicles, even in a nonspecific manner (e.g.,  $\beta$ -actin; data not shown; Taylor et al., 2011).

From the data, we sorted red-labeled proteins generally into those associated with secretory vesicles containing MMP-9 (correlation values  $>0.20$ ) and those proteins that are nonspecifically or not associated with secretory vesicles containing MMP-9 (correlation values  $<0.20$ ; Fig. 2 D). This 0.20 cutoff has previously been used to identify nonspecific or nonassociated proteins using an identical TIRF-based screen (Trexler et al., 2016). As a positive control, we determined the correlation value for MMP9-mCherry to be 0.67, which represents the highest correlated protein with MMP9-GFP. All other highly colocalized and strongly associated proteins with secretory vesicles containing MMP-9 gave correlation values ranging from  $\sim 0.50$  to 0.67. This includes proteins like calreticulin, several Rab GTPases, (e.g., Rab3D, Rab32, and both isoforms of Rab27),

iCAM-1, TIMP-1, and several other MMPs (e.g., MMP-2 and MMP-1). Moderately colocalized proteins ranged from  $\sim 0.35$  to 0.49 and include NSF,  $\alpha$ -SNAP, several VAMP proteins (e.g., VAMP8, VAMP3, and VAMP2), several MUNC proteins (e.g., MUNC13-4, MUNC13-1, and MUNC13-3), more Rabs (e.g., Rab5A, Rab40b, and Rab38) and Rab effector proteins (e.g., Rabphilin, hSlp-4, and OCRL1), and N-WASP. However, weakly colocalized proteins ranged from  $\sim 0.20$  to 0.34 and include SNAP23, hSlp-2, and several more MMPs (MMP-10 and MT1-MMP). The nonspecific or nonassociated proteins, with correlation values  $<0.20$  were numerous but include several other VAMPS (VAMP4 and VAMP7), tubulin, endophilins (endoA1 and endo A2), and the dynamins (dynamin1 and dynamin2). The complete list from the correlation analysis of secretory vesicles containing MMP9-GFP and coexpressed red-labeled proteins can be found in Table S1.

Using the three “colocalization” categories (strong, moderate, and weak; based on correlation values [ $c$ ]) allowed us to identify and rank those colocalized proteins associated with secretory vesicles containing MMP-9 (i.e., those with  $c$  values  $>0.2$ ; strong

and moderate; Fig. 2 D). We further characterized several of the highly and moderately red-labeled proteins by measuring the dynamics of these proteins at sites of exocytosis of MMP-9 in real time using TIRF. Following the classification of proteins associated with DCVs done in INS-1 cells and using this same imaging-based screening method (Trexler et al., 2016), the majority of these highly and moderately colocalized proteins identified could be subsequently grouped into four likely “functional” categories (based on roles during exocytosis): (1) proteins directly bound to secretory vesicles, including Rab GTPase and Rab effector proteins (Rabphilin, hSlp-2, hSlp-4, OCRL-1, and MUNC13-4), SNARE (SNAPs and VAMPs), and SNARE modulators; (2) proteins directly bound to the plasma membrane beneath the docked secretory vesicle, including syntaxin and MUNCs; (3) accessory proteins likely interacting with the docking complex, including complexins; and (4) other luminal secretory vesicle cargo, including MMPs, NPY, and TPA. These results suggest that a variety of proteins are colocalized with MMP-9 and could potentially be involved in its subsequent release from cells. Merged TIRF images of some of the various categories (Fig. 2 E) showed colocalization of the red-labeled proteins with secretory vesicles containing MMP9-GFP. We observed colocalization of MMP9-GFP with Rabphilin-mCherry (Rab effector proteins; Fig. 2 E, left), syntaxin13-mCherry (SNARE proteins; Fig. 2 E, middle), and MMP2-mCherry (other luminal secretory vesicle cargo; Fig. 2 E, right).

#### PMA-induced exocytic events of MMP-9 have nonuniform or heterogeneous decay kinetics

To study release of MMP-9 from secretory vesicles, we stimulated exocytosis in cells using the tumor promoter PMA (Masur et al., 1985) and imaged cells using TIRF. Consistent with previously published results (Roomi et al., 2009a,b), we showed by immunofluorescence and Western blot analysis that MCF-7 cells express basal levels of MMP-9 and are highly susceptible to PMA stimulation (Fig. S1). When we transiently expressed MMP9-GFP in MCF-7 cells, exocytosis of MMP9-GFP was rarely detected in samples without PMA treatment. However, after the addition of PMA, trafficking and robust exocytosis of MMP-9 from secretory vesicles was observed. This release of MMP-9 or fusion event was detected as a sudden sharp rise in fluorescence intensity (or a bright flash of diffraction-limited green fluorescence), followed by decay of the fluorescence signal as MMP9-GFP diffuses away from the exocytic site (Fig. 3, A and B). Using time-lapse images (Fig. 3 A), we were able to quantitate the fluorescence intensity changes that occurred at individual sites of fusion (Fig. 3 B). By monitoring the decay kinetics and averaging many fusion events at individual exocytic sites of MMP-9 from many MCF-7 cells, we were able to produce an average time-dependent decay signal associated with exocytosis of MMP-9 (Fig. 3 C). Each single fusion event was normalized so that a variety of different fusion events could be time-aligned and an average kinetic decay signal obtained (Fig. 3 D).

Because of instrument limitations and the normalization that occurs on each individual fusion event, it is difficult to determine quantitatively the absolute amplitude that results from the spike in fluorescence during exocytosis. However, since all

fusion events analyzed showed this characteristic spike, we were able to monitor the decay kinetics at individual exocytic sites of MMP9-GFP. All of the fusion events at individual exocytic sites showed nonuniform or heterogeneous decay profiles/decay kinetics (Fig. 3 D) in which cargo was released with variable kinetics and selectivity. These nonuniform (heterogeneous) decay profiles after fusion have also been observed with secretory granule cargo from a variety of other cell types and explain the large error bars in the fluorescence decay profiles we observed (Fig. 3 C). The nonuniform (heterogeneous) decay kinetics is the result of controlled release after fusion via regulating the rate or extent of fusion pore expansion (Anantharam et al., 2011; Fulop et al., 2005; Perrais et al., 2004; Taraska and Almers, 2004; Taraska et al., 2003). Using TIRF, the nonuniform decay profiles that we observed with MMP-9 release could be grouped into two types of fusion events. Some fusion events, which we refer to as type 1, were associated with vesicles that newly entered the evanescent field and fused with plasma membrane immediately without evident docking, called “newcomer/no docking” fusions (Fig. 3 D, top fusion event). Other fusion events, which we refer to as type 2, were associated with vesicles that were already docked on the plasma membrane for a period before fusion, called “predock” fusions (Fig. 3 D, bottom fusion event). Similar grouping and nomenclature have been previously reported for exocytic fusion events in insulin-secreting INS cells (Verhage and Sørensen, 2008; Yuan et al., 2015; Zhu et al., 2012). However, because of the variable fluorescence with secretory vesicles containing MMP9-GFP before fusion (Fig. 3 D) and the variable magnitude of the fusion event or spike, we were not able to unambiguously assign every decay profile to a specific type of fusion event (type 1, newcomer/no docking; or type 2, predock). Overall, these results suggest MMP9-GFP can be used to monitor regulated exocytosis in MCF-7 cells.

#### Rab GTPases and Rab effectors are lost from sites of secretory vesicles

To further study those “functional” categories of red-labeled proteins that were identified as being associated with secretory vesicles (Fig. 2 D), we monitored their dynamics at individual sites of exocytosis of MMP9-GFP, after PMA induction. By mapping the spatiotemporal coordinates of exocytic events from MMP-9 in the green channel (Fig. 4 A) onto the coexpressed red-labeled proteins, we could track the trajectories in the red channels (Fig. 4 B) at sites of fusion. Similar to what was done in the green channel (Fig. 4 C), we determined the intensity of each fluorescence signal by measuring the average fluorescence at the site of fusion, subtracting a background, and normalizing the intensity. This was done for each individual time-aligned fusion event, and then many events were averaged to produce the time-dependent changes that occurred in the red-labeled protein signal at fusion sites and release of MMP-9 (Fig. 4 D).

We chose to focus our analysis on those four functional categories (based on roles during exocytosis) that were identified as highly and moderately colocalized proteins associated with secretory vesicles containing MMP-9 (Fig. 2 D). The most abundant class of proteins that showed association ( $c > 0.20$ ) to secretory vesicles containing MMP-9 were the Rab GTPases,

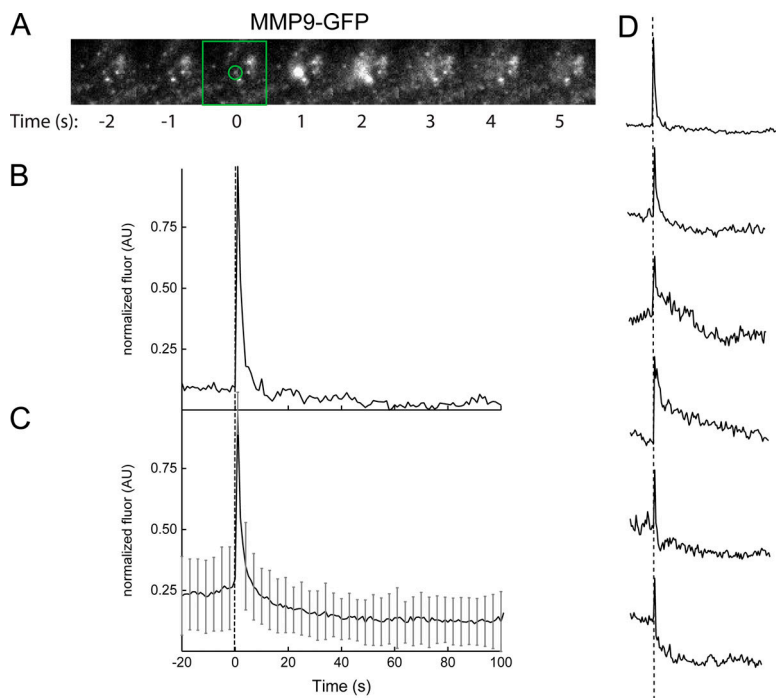


**Figure 3. Imaging of secretory vesicle fusion and exocytosis of MMP9-GFP after induction with PMA in MCF-7 cells.** (A) Snapshots of a single exocytic event over time, where the “0 s” represents the moment immediately before fusion and release of MMP9-GFP-labeled secretory vesicles. Circles ( $\sim 1 \mu\text{m}$  diameter) represent regions used for intensity analysis. (B) Time-lapse traces of normalized fluorescence signal for that one fusion event time aligned to the moment of fusion. Fluorescence (fluor) is in arbitrary units (AU). (C) Average time-lapse traces of the normalized fluorescence signal for many fusion events aligned to the moment of fusion;  $n = 72$ . Standard errors are plotted as transparent (gray) areas around the average (black) trace. (D) Representative time-lapse traces for MMP9-GFP fusion events from several exocytic sites, all time-aligned to the start of fusion (dotted line). Representative examples of type 1 and type 2 fusion events are seen in the top and bottom time-lapse traces, respectively (see Discussion).

which belongs to the functional category of proteins directly bound to secretory vesicles. Of the 24 Rabs tested, 11 were categorized as highly associated ( $c = \sim 0.50\text{--}0.67$ ) and 6 as moderately associated ( $c = \sim 0.35\text{--}0.49$ ; Fig. 2 D and Table S1). Extensive evidence has suggested that Rab-mediated vesicle trafficking and vesicle docking cooperates with oncogenic signaling pathways to promote tumorigenesis (Tzeng and Wang, 2016). Of interest were the two Rab27 isoforms (Rab27a and Rab27b) that have high correlation values. These Rab27 isoforms were of importance because both have been implicated in the late stages of exocytosis (Cazares et al., 2014), and dysregulation of both has frequently been associated with increased metastasis and tumor progression. This increase in metastasis is attributed, in part, to an increase in exocytosis of MMPs (Dong et al., 2015; Hendrix et al., 2010a, 2010b).

Specifically, we wanted to determine whether both Rab27 isoforms were required at PMA-induced exocytic sites and how the dynamics of these isoforms changed before, during, and after fusion. To this end, we generated representative time-aligned snapshots and average quantitative analysis from exocytic fusion events of MMP9-GFP in the green channel and the corresponding region in red channel for both mCherry-Rab27a (Fig. 4, A–D) and mCherry-Rab27b proteins (Fig. 4, E–H). The fluorescence trajectories in the green channels indicate that overexpression of Rab27b caused a slightly larger baseline fluorescence before fusion and release of MMP9-GFP (Fig. 4 G), as compared with overexpression of Rab27a (Fig. 4 C). Monitoring the dynamics of Rab27a and Rab27b during secretory vesicles exocytosis of MMP9-GFP revealed two important results: (1) both isoforms were localized at exocytic sites before fusion and diffused away following exocytosis (red channel; Fig. 4, B and D), and (2) both isoforms displayed nonuniform decay kinetics associated with fusion events and MMP9-GFP

release (green channel; Fig. 4, C and G). This suggests a possible source of the two different types of nonuniform (heterogeneous) decay kinetic profiles that we observed in Fig. 3 D. Since both Rab27a and Rab27b are implicated in late-stage exocytosis, we speculated that the two types of fusion events were the result of MMP-9 release through separate Rab27a- and Rab27b-dependent pathways. Overexpression of Rab27b, which resulted in a slightly larger baseline fluorescence (Fig. 4 G), is consistent with more predock fusions or type 2 fusion events. While the lower baseline fluorescence seen with overexpression of Rab27a, which had a smaller baseline fluorescence (Fig. 4 C), is consistent with more newcomer/no docking fusions or type 1 fusion events. These results suggest that both isoforms are used for vesicle trafficking and PMA-induced exocytosis of MMP-9 in nonneuronal MCF-7 cells. This result contradicts findings observed in trafficking and docking of DCVs or SLMVs in neuronal cell lines, which rely solely on the Rab27a-specific isoform for vesicle exocytosis in endocrine and neuroendocrine cells (Somasundaram and Taraska, 2018; Trexler et al., 2016). Such dual roles of Rab27-specific isoforms involvement in exocytosis have been implicated in the secretion (albeit to differing degrees) of  $\beta$ -hexosaminidase in mast cells (Singh et al., 2013). Overall, these data indicate an important role of Rab27a and Rab27b in regulated exocytosis of MMP-9 in MCF-7 cells.

We observed much faster diffusion kinetics associated with MMP-9 (Fig. 4, C and G) compared with the slower diffusion kinetics associated with the Rab27a (Fig. 4 D) and Rab27b (Fig. 4 H) proteins at sites of exocytosis tested. This difference in diffusion kinetics can be attributed to two main differences in MMP-9 and the Rab27 isoforms: (1) their association (or lack of) with the membrane before fusion (i.e., soluble, peripheral membrane, integral, or lipid-anchored proteins), and (2) their subsequent cellular environment after fusion. MMP9-GFP



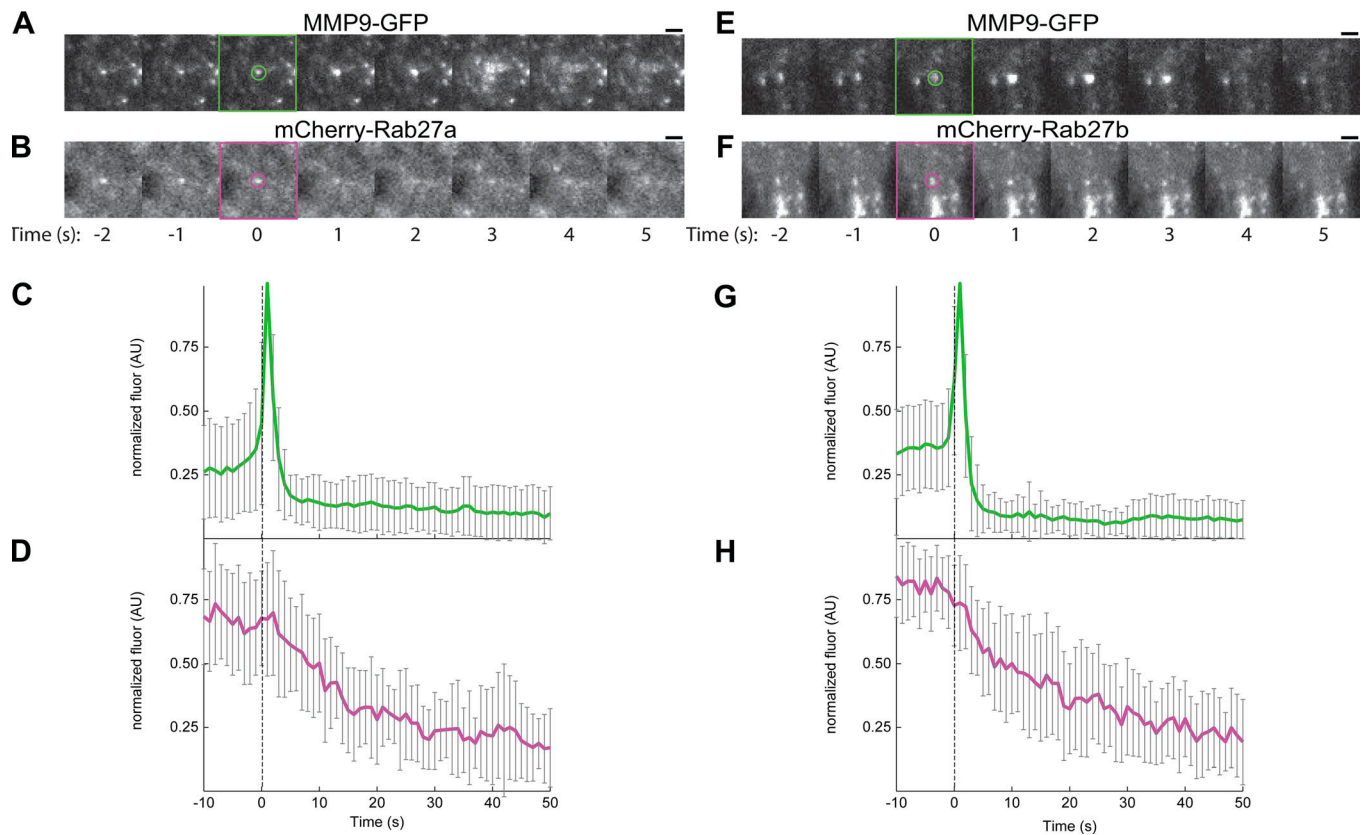


**Figure 4. Rab27a and Rab27b proteins are stably associated with secretory vesicles before exocytosis and rapidly diffuse away after exocytosis.** Gallery of representative TIRF images of MCF-7 cells transfected with MMP9-GFP and red-labeled Rab isoforms, Rab27a (A–D) and Rab27b (E–H). Shown is a fusion event in the green channel (A and E) and the corresponding region in the red channel for the Rab27 isoforms (B and F) following stimulation with PMA. Snapshots of the fusion event are at the indicated time-points. “0 s” is the manually identified first frame of brightening in the green channel. Circles (~1  $\mu\text{m}$  diameter) represent regions used for intensity analysis. Scale bar, 0.75  $\mu\text{m}$ . Average time-lapse traces of normalized fluorescence intensities for fusion events shown in the green (C and G) and red channels (D and H). Standard errors are plotted as (gray) areas around the average (green or red) trace.  $n = 50$  for Rab27a, and  $n = 33$  for Rab27b. For all exocytosis assays using two-color TIRF, 15 cells were imaged from cotransfections with the MMP-GFP and a red fluorescently labeled protein. A single coverslip with cells cotransfected with MMP9-GFP and a red-labeled protein was imaged.

showed much faster decay kinetics (Fig. 4, C and G) following secretion when compared with the slower decay kinetics of either Rab27a (Fig. 4 D) or Rab27b (Fig. 4 H) proteins diffusing away from exocytic sites following MMP-9 release. MMP-9 is a soluble protein that is stored in secretory vesicles before fusion. However, after fusion, MMP-9 is no longer restricted to secretory vesicles, and diffusion decay kinetics is fast because of the unconfined secretion of MMP-9 into an aqueous three-dimensional environment. The slower decay kinetics associated with Rab27a and Rab27b could be attributed to the fact that both Rab27 isoforms are lipid-anchored proteins, and diffusion decay kinetics is restricted to (and slowed by) the two-dimensional space of the plasma membrane.

Since we observed a role of both Rab27 isoforms (Rab27a and Rab27b) at individual exocytic sites of MMP9-GFP, we were interested in determining the behavior of several Rab27 effector proteins. There is growing evidence that suggests that multiple Rab27 effectors associated with these isoforms are involved in the regulated exocytosis of secretory granule cargo (Singh et al., 2013; Yi et al., 2002). We examined the dynamics of several Rab27 effectors proteins, including Rabphilin, hSlp-2, hSlp-4, and MUNC13-4, at individual exocytic sites of MMP-9, from

secretory vesicles. Similar to the data obtained for the Rab27 isoforms, Rabphilin, hSlp-2, and hSlp-4 were localized at exocytic sites before fusion and diffused away following exocytosis, consistent with their associations with Rab27a and Rab27b (Fig. 5, A, B, and D and Fig. S2). For these Rab27 effector proteins, we observed slow diffusion kinetics with the soluble proteins, Rabphilin and hSlp2 and with the peripheral membrane protein hSlp4. Interestingly, it seems that these soluble and peripheral Rab27 effector proteins are recruited to vesicular structures and their slow diffusion kinetics can be attributed to association with their slower lipid-anchored partners, the Rab27a and Rab27 proteins. However, unlike the other Rab27 effector proteins, the peripheral membrane protein, MUNC13-4, showed a rapid accumulation at exocytic sites near the time of fusion (Fig. 5 C).

We also examined the dynamics at fusion sites of several other Rabs that showed high colocalization with secretory vesicles containing MMP-9 (Fig. 2 D). Consistent with our finding with the Rab27 isoforms, Rab3D, Rab32, Rab25, and Rab7L1 all showed similar enrichment at exocytic sites before fusion that immediately decayed following exocytosis. This result suggests that these Rabs are all lost by diffusing away from

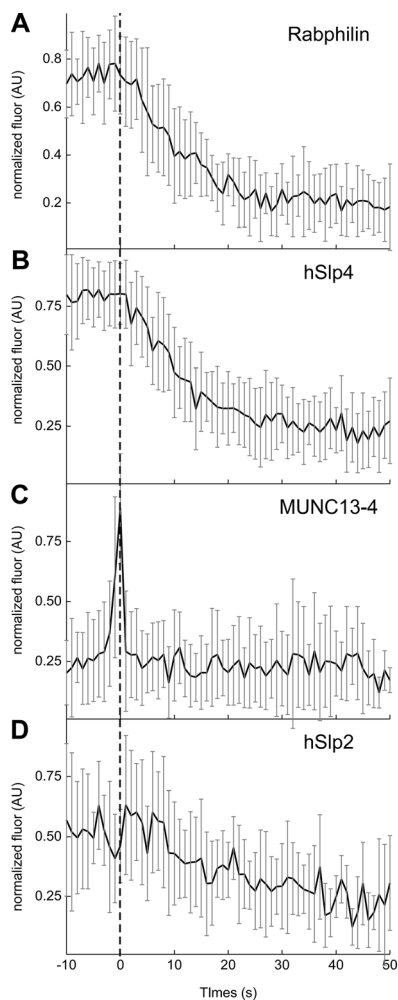


Figure 5. **Average time-lapse traces of normalized fluorescence intensity signal (dark line) of each red fluorescent protein-labeled Rab27 effector protein and the standard error of the data are shown in (gray) for all traces.**  $n = 31$  for Rabphilin (A),  $n = 30$  for hSlp4 (B),  $n = 32$  for MUNC13-4 (C), and  $n = 27$  for hSlp2 (D). Dashed line marks the zero time point that was generated from MMP9-GFP fusion event traces (green channel) and time aligned to the red channel. Background-subtracted and normalized fluorescence intensity traces are shown for each protein.

the exocytic site following MMP-9 release (Fig. 6, A–D; and Fig. S2). Additionally, all the Rabs tested (Rab3D, Rab32, Rab14, and Rab7L1; Fig. 6) showed slow diffusion decay kinetics like the Rab27 isoforms and are also classified as lipid-anchored proteins. Rab3D, the most highly correlated Rab family member associated with secretory vesicles containing MMP-9, showed some inhibitory effect on exocytosis. We observed a significantly reduced number of fusion events (10 total fusion events; Fig. 6 legend) following overexpression of Rab3D, while all other Rabs tested showed similar numbers of exocytic events (26 fusion events on average). For these exocytosis assays, we always imaged 15 cells cotransfected with MMP-GFP and a red fluorescently labeled protein. Therefore, the reduced number of fusion events suggests a possible inhibitory role of Rab3D, which was previously demonstrated when overexpression of Rab3D inhibited degranulation of  $\beta$ -hexosaminidase in mast cells (Roa

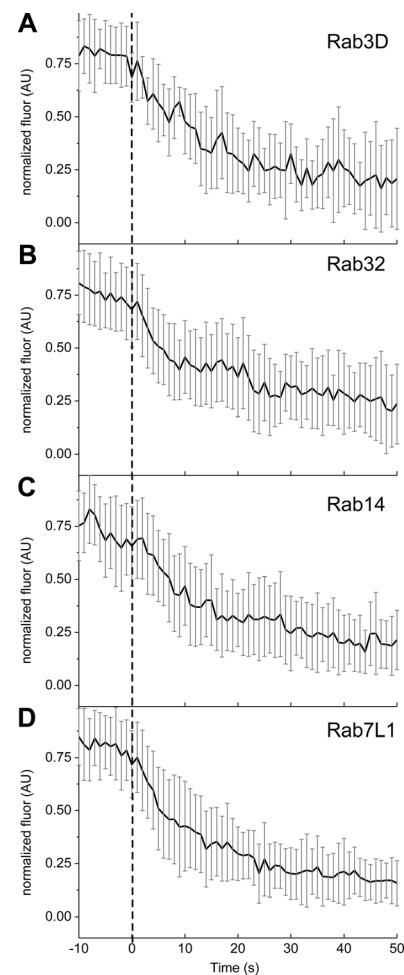


Figure 6. **Average time-lapse traces of normalized fluorescence intensity signal (dark line) of each red fluorescent protein-labeled Rab protein and the standard error of the data are shown in (gray) for all traces.**  $n = 10$  for Rab3D (A),  $n = 22$  for Rab32 (B),  $n = 28$  for Rab14 (C), and  $n = 29$  for Rab7L1 (D). Dashed line marks the zero time point that was generated from MMP9-GFP fusion event traces (green channel) and time aligned to the red channel. Background-subtracted and normalized fluorescence intensity traces are shown for each protein.

et al., 1997). More recent evidence indicates that elevated levels of Rab3D on secretory vesicles, as compared with the Rab27 isoforms in lacrimal gland acinar cells, have a negative regulatory effect on exocytosis (Meng et al., 2016). Overall, taken together, these results demonstrate that several Rab GTPase proteins and Rab effector proteins are lost from secretory vesicles following exocytosis of MMP-9.

#### SNARE and SNARE modulators exhibit a variety of effects at exocytic sites

Vesicle fusion with the plasma membrane is affected by the universal machinery known as SNARE complex (Südhof and Rizo, 2011) and includes the SNARE protein families, syntaxins, SNAPs, and VAMPs. Collectively, the SNARE proteins (and SNARE modulators), along with the small Rab family GTPases, build the core components of every membrane-trafficking event within the cell. Therefore, it was not a surprise that in addition

to the abundant number of Rabs that localized with secretory vesicles containing MMP-9, we also observed several SNARE proteins and SNARE modulators associated with these same vesicles. We categorized three SNARE proteins (VAMP8, VAMP3, and VAMP2) and three SNARE modulators (NSF, MUNC13-1, and MUNC13-3) as moderately associated ( $c = \sim 0.35\text{--}0.49$ ) and three SNARE proteins (SNAP23, VAMP4, and VAMP7) as weakly associated ( $c = \sim 0.20\text{--}0.34$ ; Fig. 2 D and Table S1).

To determine the role these proteins have at exocytic sites, we measured their dynamic behavior during fusion events of secretory vesicles with the plasma membrane and release of MMP-9. After PMA induction, the SNARE modulator, NSF (a soluble protein) and the SNARE proteins, syntaxin-13 (a single-pass IV membrane protein) and SNAP23 (a peripheral protein), all showed minor to no changes in fluorescence signal at sites of exocytosis of MMP-9 (Figs. 7 and S2). We observed the largest change in fluorescence signal from VAMP3/cellubrevin (a single-pass IV membrane protein), which showed a slow decrease in intensity following fusion (Fig. 7 B). Similarly to the Rab GTPases, VAMP3/cellubrevin slow diffusion decay kinetics could be explained by its membrane association and subsequent limited diffusion in the two-dimensional space of the plasma membrane. It is possible that overexpression of these SNARE and SNARE modulators proteins masked small changes in signal. Additionally, SNARE proteins are extremely abundant in cells, and we suspect that in general, high expression levels make it difficult to see subtle dynamic changes in their local concentration upon exocytosis (Barg et al., 2010; Knowles et al., 2010; Lang et al., 2001). Similar protein dynamics in SNARE and SNARE modulator proteins have been observed in both DCVs (Trexler et al., 2016) and SLMVs (Somasundaram and Taraska, 2018) in PC12 cells. These dynamics in protein behavior reinforce the complex spatiotemporal organization that goes into the precise timing in assembly and regulation of the exocytic machinery at sites of fusion.

### Endocytic proteins are recruited to sites of secretory vesicle exocytosis

An increasing number of studies indicate a functional link between endocytosis and exocytosis in the regulation of secretory vesicle cargo secretion (Min et al., 2007; Tsuboi et al., 2004). Localization of dynamin1 and dynamin2, classically endocytic proteins, along with the regulatory lipid phosphatidylinositol 4,5-bisphosphate (PIP2) and the dynamin-interacting proteins, endophilins and amphiphysin, have all been shown to localize to sites of exocytosis (Somasundaram and Taraska, 2018; Trexler et al., 2016). Due to the presumed role that these endocytic proteins (and regulatory lipids) have at fusion sites, we wanted to image the fluorescence changes of these proteins during the time of fusion at individual exocytic sites in MCF-7 cells. We did not observe changes in fluorescence intensity of the soluble proteins dynamin1 or dynamin2 during fusion events (Fig. 8, A and B). However, we did find that the PIP2 sensor (Fig. 8 C), along with the Bin/Amphiphysin/Rvs (BAR)-domain-containing proteins amphiphysin1 and syndapin2 (Fig. 8, D and E), are all transiently localized to exocytic sites at the moment of fusion.

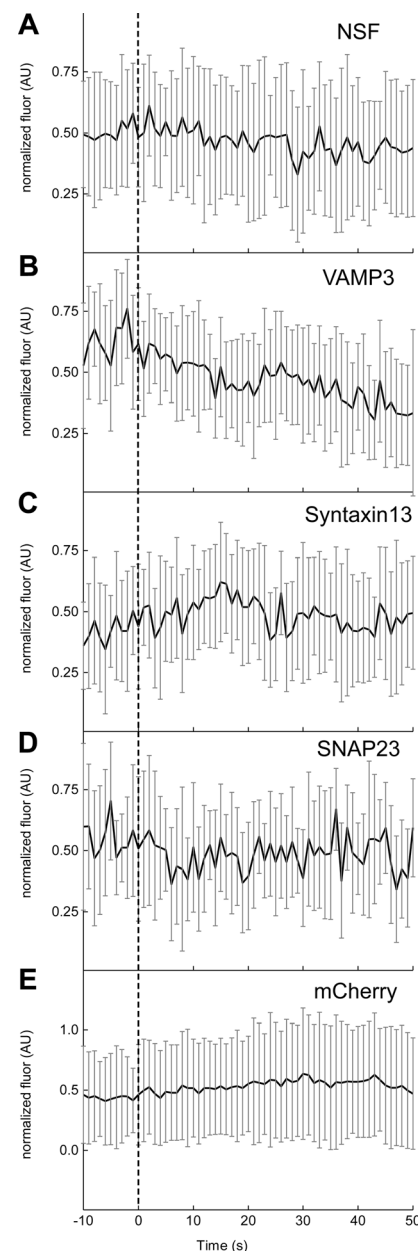


Figure 7. **Average time-lapse traces of normalized fluorescence intensity signal (dark line) of each red fluorescent protein-labeled SNARE or SNARE modulator protein and the standard error of the data are shown in gray for all traces.**  $n = 34$  for NSF (A),  $n = 17$  for VAMP3 (B),  $n = 34$  for syntaxin-13 (C),  $n = 18$  for SNAP23 (D), and  $n = 30$  for mCherry (E). Dashed line marks the zero time point that was generated from individual MMP9-GFP fusion event traces (green channel) and time aligned to the red channel. Background-subtracted and normalized fluorescence intensity traces are shown for each protein.

Although the PIP2 sensor (the  $\delta$ -domain of phospholipase C protein) and amphiphysin are soluble proteins and syndapin2 is a peripheral membrane protein, they all show an accumulation at the moment of fusion and release of MMP-9 (Fig. 8, C–E). We did not observe any accumulation of the control lipid marker farnesylated-mCherry, a lipid-anchored protein, at fusion events (Fig. 8 F). Overall, these results indicate that although the regulatory lipid PIP2 and several specific BAR-domain-containing

proteins (amphiphysin1 and syndapin2) are not needed for vesicle formation or trafficking, they are rapidly yet transiently recruited to the exocytic machinery during the moment of fusion.

### PMA-induced release of MMP-9 from secretory vesicles at single sites of fusion is associated with concurrent exocytosis of other MMPs at those same fusion sites

Cells rely on secretory vesicles for a variety of protein-associated cargo destined for exocytosis. However, how a cell distinguishes what cargo is selectively released versus retained remains unclear. Using our imaging-based screen, we identified several red-labeled cargo proteins that colocalized (high to moderate correlation values) with secretory vesicles, including NPY, TIMP1, Chromogranin A, and several other MMPs. NPY (neuropeptide) and Chromogranin A are widely used markers to visualize secretory granule exocytosis in both endocrine and many exocrine cells (including MCF-7 cells; [Desnos et al., 2007](#); [El Meskini et al., 2001a,b](#); [Jacobs et al., 2009](#)), while TIMP1 (tissue inhibitor of metalloproteinases) is a glycoprotein and a natural inhibitor of MMPs ([Gong et al., 2014](#); [Jinga et al., 2006](#)). The correlation of several other MMPs that we tested was also of importance. Among the five other MMPs tested for association with secretory vesicles containing MMP-9, two were highly correlated, including MMP-2 and MMP-1, while MMP-10 and MT1-MMP were weakly correlated ([Fig. 2 D](#)). Therefore, we focused our attention on the dynamic behavior of these highly correlated MMPs during PMA-induced exocytosis of MMP-9 in MCF-7 cells.

We first looked at MMP-2 because both MMP-2 and MMP-9 are structurally homologous and belong to the same gelatinase subgroup of MMPs. Our data indicate that during fusion events and release of MMP-9 at individual exocytic sites, there is a spike in the red fluorescence intensity consistent with an exocytic fusion event releasing MMP2-mCherry ([Fig. 9 A](#)). Interestingly, we only observed MMP-2 fusion events associated with sites that have concurrent fusion and release of MMP-9. We did not observe fusion events of MMP-2 in the absence of PMA, as was observed with MMP-9. Neither did we observe independent release of MMP-2 from sites not associated with a MMP-9 fusion event in the presence of PMA.

To confirm the TIRF imaging data showing fusion and release of MMP-2 from cells, in the absence and presence of PMA, we conducted Western blot analysis to detect MMP-2 in the conditioned media. Consistent with the live-cell imaging data, we observed an increase in secretion of MMP-2 in the conditioned media, upon PMA induction as compared with conditions without PMA ([Fig. 9, E and G](#)). Additionally, we observed fusion events causing release of MMP1-mCherry upon PMA-induction ([Fig. 9 B](#)) that were also always associated with sites of MMP-9 fusion events ([Fig. 9 D](#)). However, the release of MMP1-mCherry was not dependent on PMA induction, since we observed MMP-1 fusion events in the absence and presence of PMA, as determined by TIRF and confirmed with Western blots ([Fig. 9 F](#)). Blots for MMP-1 revealed similar levels of MMP-1 expression in the conditioned media, with or without PMA induction ([Fig. 9 G](#)). This suggests that MMP-1 secretion is not induced by PMA but is released in MCF-7 cells from the same sites of exocytosis as

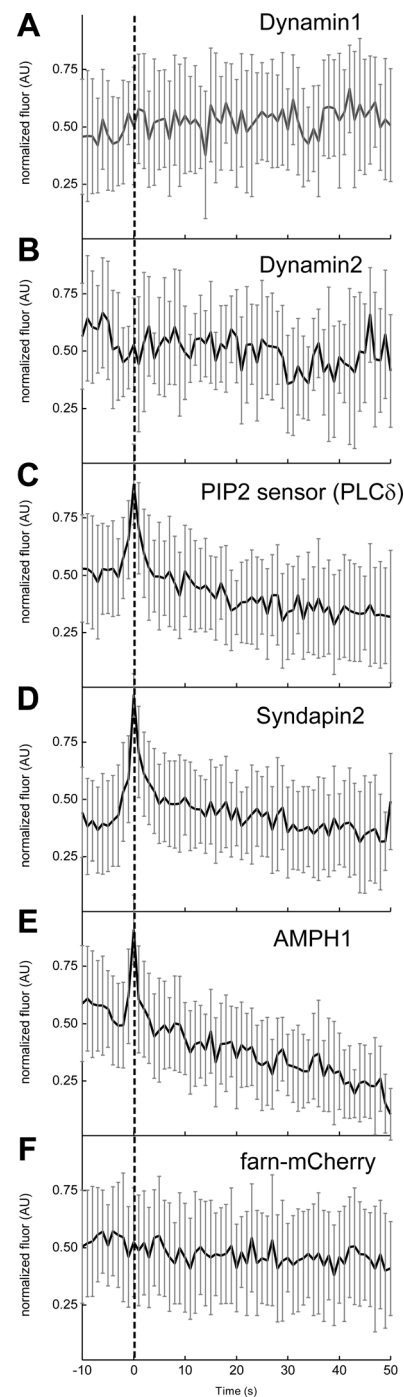
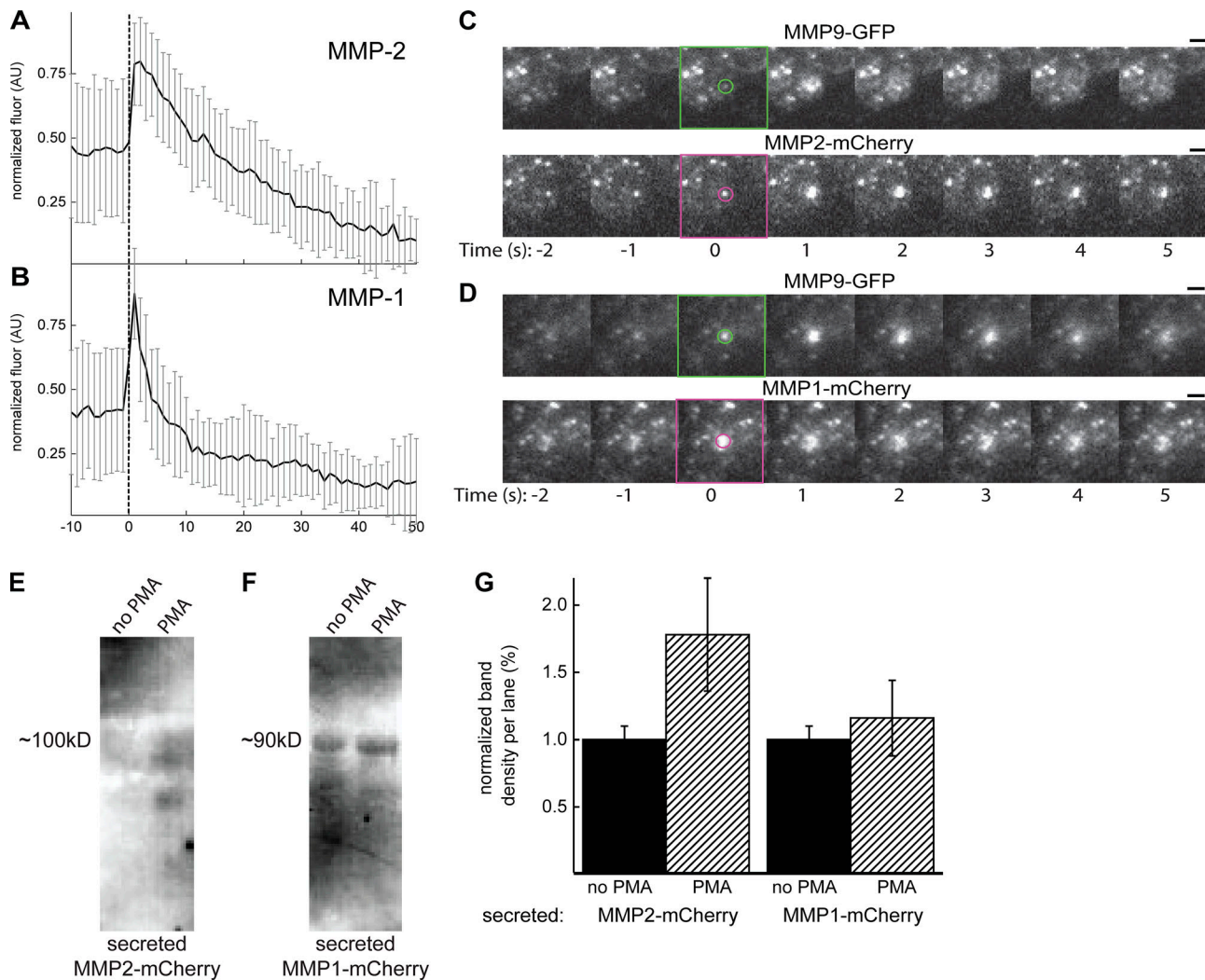


Figure 8. **Average time-lapse traces of normalized fluorescence intensity signal (dark line) of each red fluorescent protein-labeled endocytic protein and the standard error of the data are shown in (gray) for all traces.**  $n = 29$  for dynamin1 (A),  $n = 30$  for dynamin2 (B),  $n = 25$  for PIP2-sensor (C),  $n = 26$  for amphiphysin (D),  $n = 33$  for syndapin2 (E), and  $n = 32$  for farnesylated-mCherry (F). Dashed line marks the zero time point that was generated from individual MMP9-GFP fusion event traces (green channel) and time aligned to the red channel. Background-subtracted and normalized fluorescence intensity traces are shown for each protein.

MMP-9 ([Fig. 9 F](#)). Overall, these results suggest that other cargo proteins, including MMP-2 and MMP-1, use similar trafficking and exocytosis pathways as MMP-9 in MCF-7 cells.



**Figure 9. Exocytosis of MMP-9 from secretory vesicles results in concurrent release of other MMPs at those same fusion sites.** (A) Average time-lapse traces of normalized fluorescence intensities signal (dark line) of each red fluorescent protein-labeled MMP-2 protein and the standard error of the data are shown in (gray) for all traces.  $n = 25$  for MMP-2. (B) Average time-lapse traces of normalized fluorescence intensities signal (dark line) of each red fluorescent protein-labeled MMP-1 protein and the standard error of the data are shown in (gray) for all traces.  $n = 29$  for MMP-1. Dashed line marks the zero time point that was generated from individual MMP9-GFP fusion event traces (green channel) and time aligned to the red channel. Background-subtracted and normalized fluorescence intensity traces are shown for each protein. (C) Representative TIRF images of PMA-induced MCF-7 cells transfected with MMP9-GFP and red-labeled MMP2-mCherry. (D) Representative TIRF images of PMA-induced MCF-7 cells transfected with MMP9-GFP and red-labeled MMP2-mCherry. Shown is a fusion event in the green channel (upper image) and the corresponding region in the red channel (lower image) for MMP2-mCherry (C) and MMP1-mCherry (D) following stimulation with PMA. Scale bar, 0.75  $\mu\text{m}$ . (E) Western blot on conditioned media for MMP-2, without and with PMA-induction. (F) Western blot on conditioned media for MMP-1, without and with PMA-induction. (G) Quantitative densitometric analysis of MMP expression in MCF-7 cells without and with PMA. MMP expression is determined as the sum of all band densities in a given lane and reported as the average normalized band density from three independent Western blots. The error bars represent the standard error determined from averaging the normalized band density from those three independent Western blots.

For the release of either MMP-2 or MMP-1, we observed that both soluble proteins have strikingly different diffusion kinetics (Fig. 9, A and B). Although both MMP-2 and MMP-1 showed fast diffusion decay kinetics because of release into the three-dimensional aqueous media, their profiles are presumably different because of associations that MMP-2 has with the plasma membrane after fusion. MMP-2 has been localized to lipid rafts, which clusters together several degradative enzymes and proteins crucial for cancer cell migration (Patra, 2008). This suggests that the slower diffusion kinetics observed for MMP-2 (Fig. 9 A) could be due to the restricted dynamics imposed

from the outside, where MMP-2 subsequently associates with the plasma membrane. A similar recruitment of extracellular MMP-1 back to the plasma membrane has not yet been shown; therefore, the slower decay kinetics associated with MMP-1 is unclear.

**Rab27-specific isoforms are present at fusion sites and mutations alter the MMP-9 release dynamics**

Since our data indicated that exocytosis at fusion sites show differing fusion decay patterns of MMP-9 depending on which Rab27 isoform is overexpressed (Fig. 4), we imaged the behavior

of mutations to the Rab27 isoforms at individual exocytic sites. As previously shown in Fig. 4, when Rab27a- and Rab27b-specific isoforms are overexpressed in PMA-induced MCF-7 cells, we observed two distinct types of fusion decay events (i.e., type 1 or type 2 fusions) associated with MMP-9 release (green channel). The exponential fluorescence decay (with standard error) of MMP9-GFP associated with exocytic sites expressing Rab27a-WT and Rab27b-WT are  $\tau = 1.3 \pm 0.0$  s (type 1 fusion event) and  $\tau = 1.1 \pm 0.0$  s (type 2 fusion event), respectively (Fig. 10, A and B, top). We overexpressed three different mutants associated with each Rab27-specific isoform, including the Rab27 constitutively active (CA) mutant, which is defective in GTP hydrolysis (Rab27a-Q78L or Rab27b-Q78L), and Rab27 dominant-negative (DN) mutants, which are defective in GTP binding (Rab27a-T23N or Rab27b-T23N and Rab27a-N133I or Rab27b-N133I). Overexpression of either CA or DN Rab27-specific isoform mutants altered the decay kinetics associated with MMP9-GFP exocytosis by prolonging and slowing the kinetics of MMP9-GFP release from secretory vesicles, as compared with WT (Fig. 10, A and B, top). Fusion decay kinetics (with standard error) for the Rab27a mutants slowed by approximately threefold giving  $\tau = 4.2 \pm 0.2$  s (Q78L),  $\tau = 4.0 \pm 0.3$  s (N133I), and  $\tau = 3.2 \pm 0.2$  s (T23N), while Rab27b mutants slowed by approximately sixfold, giving  $\tau = 5.7 \pm 0.3$  s (Q78L),  $\tau = 7.5 \pm 0.4$  s (N133I), and  $\tau = 5.6 \pm 0.3$  s (T23N).

We also examined the protein dynamics of the Rab27-isoform-specific mutants (red channel) at these sites of exocytosis of MMP-9. When Rab27a- and Rab27b-specific isoforms are overexpressed in PMA-induced MCF-7 cells, all Rab27-specific isoform mutants for Rab27a and Rab27b still localize to sites before fusion and diffuse away following exocytosis of MMP-9, like their WT counterparts (Fig. 10, A and B, bottom). Specifically, for all of the Rab27a-specific mutations (Rab27a-Q78L, -N133I, and -T23N; Fig. 10 A, bottom), we observed a weakened or smaller change in fluorescence decay following fusion, suggesting that they may not be lost from the site of fusion as fast as in WT. For Rab27b, we observed a similar decrease in fluorescence decay associated with the DN mutant versions of Rab27b (Rab27b-N133I and Rab27b-T23N; Fig. 10 B; bottom). However, the CA mutant, Rab27b-Q78L, showed similar decay profiles to that of Rab27b-WT overexpression. These data results indicate that the GTPase activity of both Rab27-specific isoforms (Rab27a and Rab27b) may be required for their preassembly and function at exocytic sites. Collectively, the mutational analysis reinforces the possibility of two distinct types of fusion events and decay kinetics associated with the different Rab27 isoforms.

Using Western blotting, we confirmed that Rab27a and Rab27b constructs were overexpressed in transfected MCF-7 cells (Fig. S3 A). Also using Western blotting and immunofluorescence, we confirmed that both Rab27a and Rab27b isoforms were expressed in untransfected MCF-7 cells (Fig. S3 B), as previously reported (Hendrix et al., 2010a,b,c). Separate knockdown of either Rab27 isoforms using siRNA, resulted in a reduction, but not complete elimination, of Rab27a and Rab27b protein levels in cells (Fig. C). Cells transfected with MMP9-GFP and siRNA against either Rab27a or Rab27b did not affect fusion decay kinetics (Fig. S D), presumably because (1) there was

incomplete knockdown of each Rab27-specific isoform, and (2) knockdown of only one Rab27 isoform still allowed for the second Rab27 isoform for exocytosis. Since Rab27a and Rab27b are expressed by MCF-7, and both isoforms are involved in exocytosis of MMP-9, we imaged the correlation/colocalization of the two isoforms with one another. Using TIRF, we confirmed that GFP-Rab27a and mCherry-Rab27b are highly associated and colocalized (Fig. S4), having a correlation value of 0.51. The colocalization of the two Rab27 isoforms is consistent with published proteomics data of purified Rab27b secretory vesicles from MCF-7 containing an abundant amount of Rab27a (Hendrix et al., 2010c). These findings are consistent with possible distinct roles of Rab27a and Rab27b isoforms in MCF-7 cells and confirm the important role of Rab27-specific isoforms in the fusion decay kinetics associated with MMP-9 release.

## Discussion

Regulated exocytosis of secretory vesicles is a complex, dynamic, and highly coordinated process, involving a growing number of proteins and lipids interacting at sites of vesicle fusion (Jahn et al., 2003). Therefore, the spatial and temporal coordination of all these protein and lipid factors during regulated exocytosis is growing increasingly important because of their associations with many diseases, including cancer. In this study, we uncovered that the protumor marker and proteolytic enzyme MMP-9 can be used to image regulated exocytosis in MCF-7 breast adenocarcinoma cells in real time.

We confirmed that the fusion protein MMP9-GFP was expressed in secretory vesicles in MCF-7 cells (Fig. 1), identified colocalized proteins associated with the MMP9-containing secretory vesicles (Fig. 2), and monitored the dynamics associated with regulated exocytosis of MMP-9 from cells in real time (Fig. 3). Live-cell imaging of exocytosis uncovered nonuniform (heterogeneous) decay kinetics associated with individual fusion sites of the secretory vesicle marker MMP9-GFP. The nonuniform (heterogeneous) decay kinetics associated with MMP9-GFP secretion is consistent with recent evidence arguing against the traditional view that exocytosis results in uniform (homogeneous) decay kinetics and total release of granule cargo. Our data support a view of more nonuniform outcomes after fusion in which cargo is released with variable kinetics and selectivity (Rao et al., 2017; Anantharam et al., 2011; Fulop et al., 2005; Perrais et al., 2004; Taraska and Almers, 2004; Taraska et al., 2003).

We presumed that the nonuniform (or heterogeneous) decay kinetics observed at individual fusion sites during PMA-triggered MMP-9 release (Fig. 3) was the result of specific colocalized protein factors on the exocytic machinery at or near the moment of exocytosis. Therefore, the colocalized proteins that we previously identified (Fig. 2) that were of particular interest were the Rab GTPases (and Rab effector proteins), together with the SNARE proteins (and SNARE modulators), which represent the core components associated with sites of exocytosis. We first focused our attention on the Rab27 isoforms Rab27a and Rab27b because of their known involvement in late-stage exocytosis (Cazares et al., 2014). Both isoforms accumulate at fusion sites before exocytosis and are lost from the fusion site

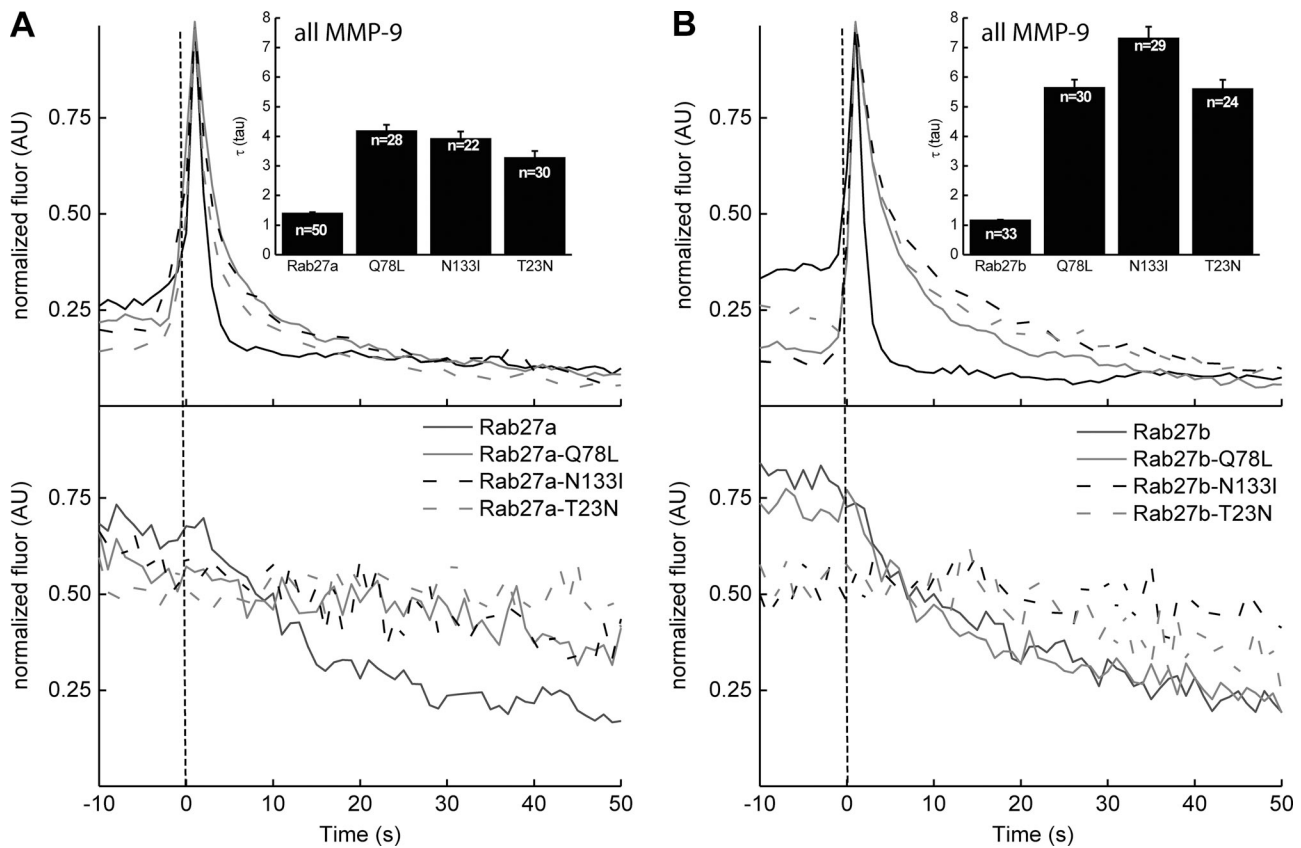


**Figure 10. Fluorescence decay kinetics of MMP-9 and Rab27-specific isoforms at fusion sites. (A)** Average time-lapse decay profiles of normalized MMP-9 fluorescence intensities (green channel) in MCF-7 cells coexpressed with Rab27a (WT) and Rab27a mutants; Rab27a-Q78L; CA (solid gray), Rab27a-N133I; DN (dashed black) and Rab27a-T23N; and DN (dashed gray). The average fusion decay kinetics and error for release of MMP9-GFP was calculated from averaging the normalized trajectories from the green channel of cells coexpressed with the mcherry-Rab27 isoforms or their mutants. **(B)** Average time-lapse decay profiles of normalized Rab27a fluorescence intensities (red channel) in same MCF-7 cells. Shown are Rab27b-WT (solid black), Rab27b-Q78L; CA (solid gray), Rab27b-N133I; DN (dashed black) and Rab27a-T23N; and DN (dashed gray). Individual event traces were time-aligned to 0 s, which corresponds to the manually identified first frame of fusion. The same dataset for Rab27a-WT and Rab27b-WT in [Figure 4](#) was used.

following exocytosis ([Fig. 4](#)). Similar dynamic behavior like that of the Rab27 isoforms was observed for several other Rabs (e.g., Rab3D, Rab32, Rab14, and Rab7L1; [Fig. 5](#)) and Rab effectors (e.g., Rabphilin, hSlp4, and hSlp2; [Fig. 6](#)) and the SNARE protein VAMP3/cellubrevin ([Fig. 7](#)). In DCVs, SLMVs, and secretory vesicles, Rab27a, Rabphilin, and VAMPs are concentrated at fusion sites and diffuse away following fusion in all three systems, supporting parallels to the molecular assembly of key components during DCV, microvesicle, and secretory vesicle exocytosis ([Larson et al., 2014; Somasundaram and Taraska, 2018; Trexler et al., 2016](#)). Overall, our data indicate a variety of dynamic behaviors of core exocytic protein components associated with the regulated release of MMP-9 from MCF-7 cells.

We also observed involvement of several classical endocytic proteins and a regulatory lipid at exocytic sites near the time of membrane fusion. Our data indicate that the lipid PIP2 and the BAR-domain proteins amphiphysin and syndapin2 are all rapidly recruited and transiently associated with exocytic sites during membrane fusion ([Fig. 8](#)). Research involving DCV fusion sites in endocrine cells and SLMV fusion sites in neuroendocrine cells showed similar dynamics for the same three factors (PIP2, amphiphysin, and syndapin2). This suggests a possible

conserved role of these proteins and lipid factors in regulating different types of vesicles and the release of their unique cargoes in a variety of cell types ([Larson et al., 2014; Somasundaram and Taraska, 2018; Trexler et al., 2016](#)). Overall, these data indicate a variety of dynamic behaviors of noncore exocytic protein components, including several classical endocytic proteins and regulatory lipids, associated with regulated exocytosis of MMP-9 from MCF-7 cells.

Additionally, we found several other MMPs are released from individual sites of exocytosis of MMP-9. Both MMP-2 and MMP-1 showed concurrent fusion events associated with sites of exocytosis of MMP-9 from secretory vesicles, but only MMP-2 was induced with PMA ([Fig. 9](#)). While MMP-1 showed similar protein levels (via Western blots) following release from MCF-7 cells, with and without stimulation by PMA, MMP-2 was only detectable (via Western blots) with PMA added. Our results with the three MMPs suggest that MMP-2 behaves more like MMP-9 than does MMP-1, based on their effects in the absence and presence of PMA. This makes sense structurally, since MMP-9 and MMP-2 are two highly homologous members of the same gelatinase subgroup of MMPs, while MMP-1 belongs to the collagenase subgrouping. These subgroupings are based partly on

historical assessment of the various substrate specificities and the cellular localization of the MMPs. Our results support the role that both cargo proteins are colocalized with secretory vesicles containing MMP-9 and are associated with concurrent release of the MMPs from the same exocytic sites. However, it is worth noting that we are unable to rule out that MMP-2 or MMP-1 overexpression might influence exocytosis of MMP-9. Overall, our finding supports the idea that a variety of MMPs inside cells have varied regulatory mechanisms controlling their release in MCF-7 cells.

Lastly, we showed that the presence of mutations in either Rab27a or Rab27b isoforms slowed the decay kinetics of MMP-9 (green channel) release following exocytosis (Fig. 10). All Rab27a and Rab27b mutants (red channel) except for CA Rab27b-Q78L diffused away and were lost from individual fusion sites more slowly than WT. This serves as a possible explanation for the slower decay kinetics associated with MMP-9 release (green channel). We hypothesize that the nonuniform (heterogeneous) fusion events or decay profiles of MMP-9 release could possibly be the result of the distinct involvements (or effects) of the two Rab27 isoforms on individual exocytic sites. On the basis of their differing effects on MMP-9 release (i.e., type 1 fusion events or type 2 fusion events; Fig. 4) and mutational effects (Fig. 10), we speculate that the two isoforms may have distinct functional roles during regulated exocytosis in MCF-7 cells. Based on the different baselines before fusion of MMP-9 that were obtained following overexpression of the two Rab27 isoforms (Fig. 10), we believe that Rab27b may have a stronger effect on docking of secretory vesicles than Rab27a in MCF-7 cells. This higher baseline fluorescence associated with Rab27b results in more predock fusions (type 2), while the lower baseline with Rab27a is consistent with more newcomer/no dock fusions (type 1). Further research will be necessary to fully understand the distinct roles that both Rab27 isoforms play at sites of exocytosis of MMP-9 from MCF-7 cells.

Overall, this work has allowed us to better understand the spatiotemporal organization of protein and lipid factors in and around individual exocytic sites of MMP-9 from MCF-7 breast cancer cells. For example, Rab27a, Rab27b, and Rab27 effector proteins are involved in assembly at fusion sites before and during exocytosis, and these components are lost from sites of exocytosis when MMP-9 is released. Our work underscores the importance of the involvement of two specific Rab27 isoforms in the late stages of exocytosis of cargo associated with secretory vesicles (e.g., MMP-9) in MCF-7 cells. Moreover, several other BAR-domain-containing proteins and lipid components, including amphiphysin, syndapin2, and PIP2, are rapidly and transiently recruited to exocytic sites near the time of membrane fusion. These factors (and others) likely modulate the fusion pore and directly regulate the release of secretory vesicle cargo, resulting in the nonuniformity or heterogeneity associated with exocytosis of MMP-9 in MCF-7 cells. Future work is necessary to understand how these factors contribute to the nonuniform fusion kinetics and the distinct types of fusion events associated with exocytosis of MMP-9 with overexpression of the Rab27-specific isoforms Rab27a and Rab27b.

## Acknowledgments

Sharona E. Gordon served as editor.

D.A. Harris is supported by the National Science Foundation (grant 1891204). J.W. Taraska is supported by the Intramural Research Program of the National Heart, Lung, and Blood Institute, National Institutes of Health.

The authors declare no competing financial interests.

Author contributions: D.A. Harris and J.W. Taraska designed the study, D.C. Stephens and D.A. Harris performed experiments, and D.C. Stephens and D.A. Harris analyzed data and wrote the manuscript.

Submitted: 22 December 2018

Accepted: 30 September 2019

## References

- Anantharam, A., M.A. Bittner, R.L. Aikman, E.L. Stuenkel, S.L. Schmid, D. Axelrod, and R.W. Holz. 2011. A new role for the dynamin GTPase in the regulation of fusion pore expansion. *Mol. Biol. Cell.* 22:1907–1918. <https://doi.org/10.1091/mbc.e11-02-0101>
- Barg, S., M.K. Knowles, X. Chen, M. Midorikawa, and W. Almers. 2010. Syntaxin clusters assemble reversibly at sites of secretory granules in live cells. *Proc. Natl. Acad. Sci. USA.* 107:20804–20809. <https://doi.org/10.1073/pnas.1014823107>
- Cazares, V.A., A. Subramani, J.J. Saldade, W. Hoerauf, and E.L. Stuenkel. 2014. Distinct actions of Rab3 and Rab27 GTPases on late stages of exocytosis of insulin. *Traffic.* 15:997–1015. <https://doi.org/10.1111/tra.12182>
- Corcoran, J.J., S.P. Wilson, and N. Kirshner. 1984. Flux of catecholamines through chromaffin vesicles in cultured bovine adrenal medullary cells. *J. Biol. Chem.* 259:6208–6214.
- Desnos, C., S. Huet, I. Fanget, C. Chapuis, C. Böttiger, V. Racine, J.B. Sibarita, J.P. Henry, and F. Darchen. 2007. Myosin va mediates docking of secretory granules at the plasma membrane. *J. Neurosci.* 27:10636–10645. <https://doi.org/10.1523/JNEUROSCI.1228-07.2007>
- Dong, W., J. Cui, J. Yang, W. Li, S. Wang, X. Wang, X. Li, Y. Lu, and W. Xiao. 2015. Decreased expression of Rab27A and Rab27B correlates with metastasis and poor prognosis in colorectal cancer. *Discov. Med.* 20:357–367.
- El Meskini, R., G.J. Galano, R. Marx, R.E. Mains, and B.A. Eipper. 2001a. Targeting of membrane proteins to the regulated secretory pathway in anterior pituitary endocrine cells. *J. Biol. Chem.* 276:3384–3393. <https://doi.org/10.1074/jbc.M008062200>
- El Meskini, R., L. Jin, R. Marx, A. Bruzzaniti, J. Lee, R. Emeson, and R. Mains. 2001b. A signal sequence is sufficient for green fluorescent protein to be routed to regulated secretory granules. *Endocrinology.* 142:864–873. <https://doi.org/10.1210/endo.142.2.7929>
- Fulop, T., S. Radabaugh, and C. Smith. 2005. Activity-dependent differential transmitter release in mouse adrenal chromaffin cells. *J. Neurosci.* 25:7324–7332. <https://doi.org/10.1523/JNEUROSCI.2042-05.2005>
- Gomi, H., K. Mori, S. Itohara, and T. Izumi. 2007. Rab27b is expressed in a wide range of exocytic cells and involved in the delivery of secretory granules near the plasma membrane. *Mol. Biol. Cell.* 18:4377–4386. <https://doi.org/10.1091/mbc.e07-05-0409>
- Gong, Y., U.D. Chippada-Venkata, and W.K. Oh. 2014. Roles of matrix metalloproteinases and their natural inhibitors in prostate cancer progression. *Cancers (Basel).* 6:1298–1327. <https://doi.org/10.3390/cancers6031298>
- Graczyk, A., and C. Rickman. 2013. Exocytosis through the Lens. *Front. Endocrinol. (Lausanne).* 4:147. <https://doi.org/10.3389/fendo.2013.00147>
- Haferlach, T., A. Köhlmann, L. Wiczorek, G. Basso, G.T. Kronnie, M.C. Béné, J. De Vos, J.M. Hernández, W.K. Hofmann, K.I. Mills, et al. 2010. Clinical utility of microarray-based gene expression profiling in the diagnosis and subclassification of leukemia: report from the International Microarray Innovations in Leukemia Study Group. *J. Clin. Oncol.* 28:2529–2537. <https://doi.org/10.1200/JCO.2009.23.4732>
- Hendrix, A., G. Braems, M. Bracke, M. Seabra, W. Gahl, O. De Wever, and W. Westbroek. 2010a. The secretory small GTPase Rab27B as a marker for breast cancer progression. *Oncotarget.* 1:304–308. <https://doi.org/10.18632/oncotarget.140>



- Hendrix, A., D. Maynard, P. Pauwels, G. Braems, H. Denys, R. Van den Broecke, J. Lambert, S. Van Belle, V. Cocquyt, C. Gespach, et al. 2010b. Effect of the secretory small GTPase Rab27B on breast cancer growth, invasion, and metastasis. *J. Natl. Cancer Inst.* 102:866–880. <https://doi.org/10.1093/jnci/djq153>
- Hendrix, A., W. Westbroek, M. Bracke, and O. De Wever. 2010c. An ex(o) citing machinery for invasive tumor growth. *Cancer Res.* 70:9533–9537. <https://doi.org/10.1158/0008-5472.CAN-10-3248>
- Heuser, J. 2000. The production of ‘cell cortices’ for light and electron microscopy. *Traffic.* 1:545–552. <https://doi.org/10.1034/j.1600-0854.2000.010704.x>
- Jacobs, D.T., R. Weigert, K.D. Grode, J.G. Donaldson, and R.E. Cheney. 2009. Myosin Vc is a molecular motor that functions in secretory granule trafficking. *Mol. Biol. Cell.* 20:4471–4488. <https://doi.org/10.1091/mbc.e08-08-0865>
- Jahn, R., and D. Fasshauer. 2012. Molecular machines governing exocytosis of synaptic vesicles. *Nature.* 490:201–207. <https://doi.org/10.1038/nature11320>
- Jahn, R., T. Lang, and T.C. Südhof. 2003. Membrane fusion. *Cell.* 112:519–533. [https://doi.org/10.1016/S0092-8674\(03\)00112-0](https://doi.org/10.1016/S0092-8674(03)00112-0)
- Jinga, D.C., A. Blidaru, I. Condrea, C. Ardeleanu, C. Dragomir, G. Szegli, M. Stefanescu, and C. Matache. 2006. MMP-9 and MMP-2 gelatinases and TIMP-1 and TIMP-2 inhibitors in breast cancer: correlations with prognostic factors. *J. Cell. Mol. Med.* 10:499–510. <https://doi.org/10.1111/j.1582-4934.2006.tb00415.x>
- Kean, M.J., K.C. Williams, M. Skalski, D. Myers, A. Burtnik, D. Foster, and M.G. Coppelino. 2009. VAMP3, syntaxin-13 and SNAP23 are involved in secretion of matrix metalloproteinases, degradation of the extracellular matrix and cell invasion. *J. Cell Sci.* 122:4089–4098. <https://doi.org/10.1242/jcs.052761>
- Knowles, M.K., S. Barg, L. Wan, M. Midorikawa, X. Chen, and W. Almers. 2010. Single secretory granules of live cells recruit syntaxin-1 and synaptosomal associated protein 25 (SNAP-25) in large copy numbers. *Proc. Natl. Acad. Sci. USA.* 107:20810–20815. <https://doi.org/10.1073/pnas.1014840107>
- Lang, T., D. Bruns, D. Wenzel, D. Riedel, P. Holroyd, C. Thiele, and R. Jahn. 2001. SNAREs are concentrated in cholesterol-dependent clusters that define docking and fusion sites for exocytosis. *EMBO J.* 20:2202–2213. <https://doi.org/10.1093/emboj/20.9.2202>
- Larson, B.T., K.A. Sochacki, J.M. Kindem, and J.W. Taraska. 2014. Systematic spatial mapping of proteins at exocytic and endocytic structures. *Mol. Biol. Cell.* 25:2084–2093. <https://doi.org/10.1091/mbc.e14-02-0771>
- Llobet, A., M. Wu, and L. Lagnado. 2008. The mouth of a dense-core vesicle opens and closes in a concerted action regulated by calcium and amphiphysin. *J. Cell Biol.* 182:1017–1028. <https://doi.org/10.1083/jcb.200807034>
- Lu, P., K. Takai, V.M. Weaver, and Z. Werb. 2011. Extracellular matrix degradation and remodeling in development and disease. *Cold Spring Harb. Perspect. Biol.* 3:a005058. <https://doi.org/10.1101/cshperspect.a005058>
- Masur, S.K., V. Sapirstein, and D. Rivero. 1985. Phorbol myristate acetate induces endocytosis as well as exocytosis and hydroosmosis in toad urinary bladder. *Biochim. Biophys. Acta.* 821:286–296. [https://doi.org/10.1016/0005-2736\(85\)90098-7](https://doi.org/10.1016/0005-2736(85)90098-7)
- Mendes, O., H.T. Kim, and G. Stoica. 2005. Expression of MMP2, MMP9 and MMP3 in breast cancer brain metastasis in a rat model. *Clin. Exp. Metastasis.* 22:237–246. <https://doi.org/10.1007/s10585-005-8115-6>
- Meng, Z., M.C. Edman, P.Y. Hsueh, C.Y. Chen, W. Klinggam, T. Tolmacheva, C.T. Okamoto, and S.F. Hamm-Alvarez. 2016. Imbalanced Rab3D versus Rab27 increases cathepsin S secretion from lacrimal acini in a mouse model of Sjögren’s Syndrome. *Am. J. Physiol. Cell Physiol.* 310:C942–C954. <https://doi.org/10.1152/ajpcell.00275.2015>
- Min, L., Y.M. Leung, A. Tomas, R.T. Watson, H.Y. Gaisano, P.A. Halban, J.E. Pessin, and J.C. Hou. 2007. Dynammin is functionally coupled to insulin granule exocytosis. *J. Biol. Chem.* 282:33530–33536. <https://doi.org/10.1074/jbc.M703402200>
- Patra, S.K. 2008. Dissecting lipid raft facilitated cell signaling pathways in cancer. *Biochim. Biophys. Acta.* 1785:182–206.
- Perrais, D., I.C. Kleppe, J.W. Taraska, and W. Almers. 2004. Recapture after exocytosis causes differential retention of protein in granules of bovine chromaffin cells. *J. Physiol.* 560:413–428. <https://doi.org/10.1113/jphysiol.2004.064410>
- Ran, F.A., P.D. Hsu, C.Y. Lin, J.S. Gootenberg, S. Konermann, A.E. Trevino, D.A. Scott, A. Inoue, S. Matoba, Y. Zhang, and F. Zhang. 2013a. Double nicking by RNA-guided CRISPR Cas9 for enhanced genome editing specificity. *Cell.* 154:1380–1389. <https://doi.org/10.1016/j.cell.2013.08.021>
- Ran, F.A., P.D. Hsu, J. Wright, V. Agarwala, D.A. Scott, and F. Zhang. 2013b. Genome engineering using the CRISPR-Cas9 system. *Nat. Protoc.* 8:2281–2308. <https://doi.org/10.1038/nprot.2013.143>
- Rao, T.C., Z. Santana Rodriguez, M.M. Bradberry, A.H. Ranski, P.J. Dahl, M.W. Schmidtke, P.M. Jenkins, D. Axelrod, E.R. Chapman, D.R. Giovannucci, and A. Anantharam. 2017. Synaptotagmin isoforms confer distinct activation kinetics and dynamics to chromaffin cell granules. *J. Gen. Physiol.* 149:763–780. <https://doi.org/10.1085/jgp.201711757>
- Roa, M., F. Paumet, J. Le Mao, B. David, and U. Blank. 1997. Involvement of the ras-like GTPase rab3d in RBL-2H3 mast cell exocytosis following stimulation via high affinity IgE receptors (Fc epsilonRI). *J. Immunol.* 159:2815–2823.
- Roomi, M.W., J.C. Monterrey, T. Kalinovsky, M. Rath, and A. Niedzwiecki. 2009a. Distinct patterns of matrix metalloproteinase-2 and -9 expression in normal human cell lines. *Oncol. Rep.* 21:821–826.
- Roomi, M.W., J.C. Monterrey, T. Kalinovsky, M. Rath, and A. Niedzwiecki. 2009b. Patterns of MMP-2 and MMP-9 expression in human cancer cell lines. *Oncol. Rep.* 21:1323–1333.
- Saito, T., H. Mizumoto, R. Tanaka, S. Satohisa, K. Adachi, M. Horie, and R. Kudo. 2004. Overexpressed progesterone receptor form B inhibit invasive activity suppressing matrix metalloproteinases in endometrial carcinoma cells. *Cancer Lett.* 209:237–243. <https://doi.org/10.1016/j.canlet.2003.12.017>
- Sakata, K., M. Satoh, M. Someya, H. Asanuma, H. Nagakura, A. Oouchi, K. Nakata, K. Kogawa, K. Koito, M. Hareyama, and T. Himi. 2004. Expression of matrix metalloproteinase 9 is a prognostic factor in patients with non-Hodgkin lymphoma. *Cancer.* 100:356–365. <https://doi.org/10.1002/cncr.11905>
- Samasilp, P., S.A. Chan, and C. Smith. 2012. Activity-dependent fusion pore expansion regulated by a calcineurin-dependent dynamin-syndapin pathway in mouse adrenal chromaffin cells. *J. Neurosci.* 32:10438–10447. <https://doi.org/10.1523/JNEUROSCI.1299-12.2012>
- Schnaeker, E.M., R. Ossig, T. Ludwig, R. Dreier, H. Oberleithner, M. Wilhelm, and S.W. Schneider. 2004. Microtubule-dependent matrix metalloproteinase-2/matrix metalloproteinase-9 exocytosis: prerequisite in human melanoma cell invasion. *Cancer Res.* 64:8924–8931. <https://doi.org/10.1158/0008-5472.CAN-04-0324>
- Seftor, R.E., E.A. Seftor, N. Koshikawa, P.S. Meltzer, L.M. Gardner, M. Bilban, W.G. Stetler-Stevenson, V. Quaranta, and M.J. Hendrix. 2001. Cooperative interactions of laminin 5 gamma2 chain, matrix metalloproteinase-2, and membrane type-1-matrix/metalloproteinase are required for mimicry of embryonic vasculogenesis by aggressive melanoma. *Cancer Res.* 61:6322–6327.
- Shaughnessy, R., and A. Echard. 2018. Rab35 GTPase and cancer: Linking membrane trafficking to tumorigenesis. *Traffic.* 19:247–252. <https://doi.org/10.1111/tra.12546>
- Singh, R.K., K. Mizuno, C. Wasmeier, S.T. Wavre-Shapton, C. Recchi, S.D. Catz, C. Futter, T. Tolmacheva, A.N. Hume, and M.C. Seabra. 2013. Distinct and opposing roles for Rab27a/Mlph/MyoVa and Rab27b/Munc13-4 in mast cell secretion. *FEBS J.* 280:892–903.
- Singh, D., S.K. Srivastava, T.K. Chaudhuri, and G. Upadhyay. 2015. Multifaceted role of matrix metalloproteinases (MMPs). *Front. Mol. Biosci.* 2:19. <https://doi.org/10.3389/fmolb.2015.00019>
- Sochacki, K.A., B.T. Larson, D.C. Sengupta, M.P. Daniels, G. Shtengel, H.F. Hess, and J.W. Taraska. 2012. Imaging the post-fusion release and capture of a vesicle membrane protein. *Nat. Commun.* 3:1154. <https://doi.org/10.1038/ncomms2158>
- Somasundaram, A., and J.W. Taraska. 2018. Local protein dynamics during microvesicle exocytosis in neuroendocrine cells. *Mol. Biol. Cell.* 29:1891–1903. <https://doi.org/10.1091/mbc.E17-12-0716>
- Stetler-Stevenson, W.G. 2001. The role of matrix metalloproteinases in tumor invasion, metastasis, and angiogenesis. *Surg. Oncol. Clin. N. Am.* 10:383–392. [https://doi.org/10.1016/S1055-3207\(18\)30071-1](https://doi.org/10.1016/S1055-3207(18)30071-1)
- Stetler-Stevenson, W.G., and A.E. Yu. 2001. Proteases in invasion: matrix metalloproteinases. *Semin. Cancer Biol.* 11:143–152. <https://doi.org/10.1006/scbi.2000.0365>
- Sudhof, T.C. 2004. The synaptic vesicle cycle. *Annu. Rev. Neurosci.* 27:509–547. <https://doi.org/10.1146/annurev.neuro.26.041002.131412>
- Südhof, T.C., and J. Rizo. 2011. Synaptic vesicle exocytosis. *Cold Spring Harb. Perspect. Biol.* 3:3. <https://doi.org/10.1101/cshperspect.a005637>
- Sun, Q., X. Huang, Q. Zhang, J. Qu, Y. Shen, X. Wang, H. Sun, J. Wang, L. Xu, X. Chen, and B. Ren. 2016. SNAP23 promotes the malignant process of ovarian cancer. *J. Ovarian Res.* 9:80. <https://doi.org/10.1186/s13048-016-0289-9>
- Taraska, J.W., and W. Almers. 2004. Bilayers merge even when exocytosis is transient. *Proc. Natl. Acad. Sci. USA.* 101:8780–8785. <https://doi.org/10.1073/pnas.0401316101>

- Taraska, J.W., D. Perrais, M. Ohara-Imaizumi, S. Nagamatsu, and W. Almers. 2003. Secretory granules are recaptured largely intact after stimulated exocytosis in cultured endocrine cells. *Proc. Natl. Acad. Sci. USA.* 100: 2070–2075. <https://doi.org/10.1073/pnas.0337526100>
- Taylor, M.J., D. Perrais, and C.J. Merrifield. 2011. A high precision survey of the molecular dynamics of mammalian clathrin-mediated endocytosis. *PLoS Biol.* 9:e1000604. <https://doi.org/10.1371/journal.pbio.1000604>
- Trexler, A.J., K.A. Sochacki, and J.W. Taraska. 2016. Imaging the recruitment and loss of proteins and lipids at single sites of calcium-triggered exocytosis. *Mol. Biol. Cell.* 27:2423–2434. <https://doi.org/10.1091/mbc.e16-01-0057>
- Tsuboi, T., H.T. McMahon, and G.A. Rutter. 2004. Mechanisms of dense core vesicle recapture following “kiss and run” (“cavcapture”) exocytosis in insulin-secreting cells. *J. Biol. Chem.* 279:47115–47124. <https://doi.org/10.1074/jbc.M408179200>
- Tzeng, H.T., and Y.C. Wang. 2016. Rab-mediated vesicle trafficking in cancer. *J. Biomed. Sci.* 23:70. <https://doi.org/10.1186/s12929-016-0287-7>
- Tzeng, H.T., C.H. Tsai, Y.T. Yen, H.C. Cheng, Y.C. Chen, S.W. Pu, Y.S. Wang, Y.S. Shan, Y.L. Tseng, W.C. Su, et al. 2017. Dysregulation of Rab37-Mediated Cross-talk between Cancer Cells and Endothelial Cells via Thrombospondin-1 Promotes Tumor Neovasculature and Metastasis. *Clin. Cancer Res.* 23:2335–2345. <https://doi.org/10.1158/1078-0432.CCR-16-1520>
- Verhage, M., and J.B. Sørensen. 2008. Vesicle docking in regulated exocytosis. *Traffic.* 9:1414–1424. <https://doi.org/10.1111/j.1600-0854.2008.00759.x>
- Vic, P., F. Vignon, D. Derocq, and H. Rochefort. 1982. Effect of estradiol on the ultrastructure of the MCF7 human breast cancer cells in culture. *Cancer Res.* 42:667–673.
- Wang, S., C. Hu, F. Wu, and S. He. 2017. Rab25 GTPase: Functional roles in cancer. *Oncotarget.* 8:64591–64599.
- Weigelt, B., J.L. Peterse, and L.J. van't Veer. 2005. Breast cancer metastasis: markers and models. *Nat. Rev. Cancer.* 5:591–602. <https://doi.org/10.1038/nrc1670>
- Williams, K.C., R.E. McNeilly, and M.G. Coppelino. 2014. SNAP23, Syntaxin4, and vesicle-associated membrane protein 7 (VAMP7) mediate trafficking of membrane type 1-matrix metalloproteinase (MT1-MMP) during invadopodium formation and tumor cell invasion. *Mol. Biol. Cell.* 25: 2061–2070. <https://doi.org/10.1091/mbc.e13-10-0582>
- Yi, Z., H. Yokota, S. Torii, T. Aoki, M. Hosaka, S. Zhao, K. Takata, T. Takeuchi, and T. Izumi. 2002. The Rab27a/granophilin complex regulates the exocytosis of insulin-containing dense-core granules. *Mol. Cell. Biol.* 22: 1858–1867. <https://doi.org/10.1128/MCB.22.6.1858-1867.2002>
- Yuan, T., J. Lu, J. Zhang, Y. Zhang, and L. Chen. 2015. Spatiotemporal detection and analysis of exocytosis reveal fusion “hotspots” organized by the cytoskeleton in endocrine cells. *Biophys. J.* 108:251–260. <https://doi.org/10.1016/j.bpj.2014.11.3462>
- Zhang, B., L. Yan, P.C. Tsang, and M.A. Moses. 2005. Matrix metalloproteinase-2 (MMP-2) expression and regulation by tumor necrosis factor alpha (TNFalpha) in the bovine corpus luteum. *Mol. Reprod. Dev.* 70:122–132. <https://doi.org/10.1002/mrd.20196>
- Zhu, D., Y. Zhang, P.P. Lam, S. Dolai, Y. Liu, E.P. Cai, D. Choi, S.A. Schroer, Y. Kang, E.M. Allister, et al. 2012. Dual role of VAMP8 in regulating insulin exocytosis and islet  $\beta$  cell growth. *Cell Metab.* 16:238–249. <https://doi.org/10.1016/j.cmet.2012.07.001>